Inorg. Chem. **2003**, *42*, 4366–4381

Electronic Structures of Mixed-Sandwich Complexes of Cyclopentadienyl and Hydrotris(pyrazolyl)borate Ligands with 3d Transition Metals

Tim J. Brunker, Jennifer C. Green, and Dermot O'Hare*

Inorganic Chemistry Laboratory, South Parks Road, Oxford, OX1 3QR, U.K.

Received February 20, 2003

The electronic and magnetic properties of a series of mixed-sandwich complexes MCp^RTp (Cp^R = Cp or Cp*; Tp = hydrotris(pyrazolyl)borate; M = V, Cr, Fe, Co or Ni) have been studied and compared to their homoleptic analogues, MCp^R_2 and MTp_2. Solid-state magnetic susceptibility measurements and EPR spectroscopic data indicate that complexes with d^3, d^6, and d^8 configurations are similar electronically to their metallocene analogues, except for FeCp*Tp, which displays a spin equilibrium ($S = 0 \Leftrightarrow S = 2$) in solution which was investigated by variable-temperature NMR spectroscopy. The d^2 complex $[VCpTp]^+$ displays magnetic behavior consistent with an orbitally nondegenerate ground state. The d^4 species CrCp*Tp has a high-spin ($S = 2$) ground state. The d^7 species CoCpTp is high spin ($S = 3/2$) whereas its Cp* analogue and $[NiCp^*Tp]^+$ are both low-spin ($S = 1/2$) species. The optical spectra of the d^3, d^6, and d^8 complexes were assigned in a fashion similar to the analogous metallocenes and ligand-field parameters ($\Delta_1 = \delta$-σ gap, $\Delta_2 = \sigma$-π gap for d-orbitals in axial symmetry) calculated. The analysis shows that for 15-electron species the total ligand-field splitting, Δ_{TOT}, is larger than for their metallocene analogues, whereas for the 18-electron case Δ_{TOT} is smaller and for 20-electron systems Δ_{TOT} is approximately the same. In all cases Δ_2 is substantially reduced compared to the metallocenes, and in the majority of cases Δ_1 is markedly larger. DFT calculations were performed to investigate further the nature of the ligand environment on the frontier orbitals in these complexes. Orbital energies and compositions were calculated and compared for a series of homoleptic and mixed-sandwich complexes of Ni(II) and across the 1st transition series for MCp^RTp species. The ability of Tp (vs Cp) to act as a δ-donor (with respect to the principal molecular axis) imparts significant ligand antibonding character to the δ-orbitals and results in decreased ϵ_π-ϵ_δ values compared to the metallocenes and an increased tendency toward high-spin complexes in the mixed-sandwich complexes. Structure calculations were performed for CrCp*Tp, $[VCpTp]^+$, and CoCp*Tp which show substantial distortions from ideal axial symmetry in their crystal structures. The origins of these distortions were confirmed to arise from unequal occupancy of near-degenerate δ- and π-levels.

Introduction

We have been investigating the chemistry of "mixed-sandwich" complexes containing a Cp or Cp* and a Tp (or Tpm) ligand bound to the same metal center[1] and have previously reported on the synthesis and structures of a series of such complexes with a range of first-row transition metals (V, Cr, Fe, Co, and Ni; see Figure 1).[2] A strong motivation for this work was a comparison of the properties of these molecules with their homoleptic analogues, the metallocenes and MTp_2 complexes: our previous report provided a comparison of some electrochemical, structural and reactivity properties of these compounds. In this paper we report in greater detail the magnetic data (susceptibility measurements and EPR spectroscopy) and electronic spectra of these compounds, as well as some density functional theory (DFT) calculations, to gain greater insight into their electronic structures. Some of this work has appeared in preliminary form.[3,4]

The analogous, anionic six-electron donor ligands Tp and Cp feature very prominently in transition metal chemistry.

* To whom correspondence should be addresssed. E-mail: dermot.ohare@chem.ox.ac.uk.

(1) Abbreviations: Cp = C_5H_5; Cp* = C_5Me_5; Cp^R = general substituted Cp ligand; Tp = hydrotris(pyrazolyl)borate; Tpm = hydrotris-(pyrazolyl)methane.

(2) Brunker, T. J.; Cowley, A. R.; O'Hare, D. *Organometallics* **2002**, *21*, 3123−3138.

10.1021/ic030073u CCC: $25.00
Published on Web 06/10/2003

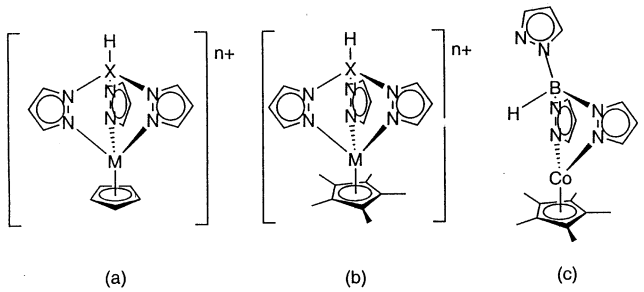

Figure 1. Mixed-sandwich complexes discussed in this work of (a) Cp and X = B, Tp (where $n = 0$, M = V, Co, Ni; where $n = 1$, M = V, Co) and X = C, Tpm (where $n = 1$ and 2, M = Co), (b) Cp* and X = B, Tp (where $n = 0$, M = Cr, Fe, Ni; where $n = 1$, M = Cr, Co, Ni) and X = C, Tpm (where $n = 1$ and M = Fe), and (c) solid-state structure of CoCp*Tp.

Significant differences in the nature of the bonding between each ligand and a metal center however results in substantial changes in the properties and reactivity of analogous complexes.[5] Tp is a tripodal hard N-donor ligand, while Cp is a softer binding ligand through the aromatic π-system.[6] However, Tp is a weak-field ligand, as evidenced by the high-spin behavior of many MTp_2 complexes,[7] while Cp is an intermediate-field ligand forming mostly low-spin complexes.[8] The metallocenes themselves have been much studied by a wide range of physical techniques, and the bonding is now well understood.[9−11] MTp_2 complexes have received somewhat less comprehensive study but include detailed optical and EPR analyses,[7,12,13] studies of the spin-crossover behavior in the Fe(II) species,[14−18] and photoelectron spectroscopy studies.[19,20]

The MO scheme for each complex type shows the splitting of the d-based orbitals into three sets, which can be classified by their symmetry with respect to the principal molecular axis: the high energy antibonding π-orbitals ($2e_g$ in D_{3d} symmetry for MTp_2, e_{1g} for a D_{5d} metallocene); a weakly bonding σ-orbital (a_{1g} in both cases); nonbonding (or slightly back-bonding in MCp_2) δ-orbitals (e_g in D_{3d}, e_{2g} in D_{5d}) (as shown in Figure 2). The splittings between these levels account for the magnetic properties in each complex type, with Δ_2 being larger for the metallocenes and small Δ_1 splittings in both cases. The relative ordering of the σ- and δ-orbitals has been a matter of some debate for MCp_2 species. We can envisage a similar bonding picture for the mixed-sandwich species. Although the formal symmetry of a symmetrically bound MCpTp complex is C_s (containing only a mirror-plane symmetry element), it can be regarded as having effective C_{3v} symmetry by comparison with other $CpML_3$ complexes.[21] Thus, the d orbitals split as a_1, 1e, and 2e (equivalent to σ, δ, and π, respectively, in axial symmetry); however, we would expect the Cp/Tp combination to generate somewhat different ligand-field splittings from either homoleptic case. Initially therefore we measured the magnetic properties to derive information about the ground-state electronic configurations in these species.

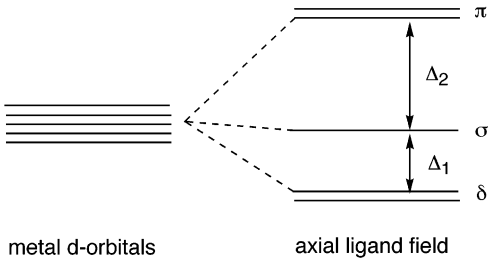

Figure 2. d-orbital splitting pattern in an axially symmetric ligand field.

Results and Discussion

Magnetic Properties of Mixed-Sandwich Complexes MCp^RTp (M = V, Cr, Fe, Co, and Ni). d^2 Species. Very few axially symmetric 14-electron metallocene (d^2) species are known, and those that exist are found mainly with Ti(II). "Titanocene" itself is not a simple sandwich complex but is found as several dimeric isomers with hydride bridges enabling a 16-electron configuration.[22,23] $TiCp^*_2$ is stable as a solid but exists in equilibrium in solution with a 16-electron isomer, $TiCp^*(\eta^6\text{-}C_5Me_4CH_2)H$. It is paramagnetic, although measurements of the moment give values significantly reduced from the spin-only value for two unpaired electrons (2.83 μ_B).[24,25] Recently, two stable monomeric titanocenes have been reported with bulky Cp ligands: $Ti\{C_5Me_4(SiMe_2Bu^t)\}_2$ is reported to have a solution moment of 2.4 μ_B,[26]

(3) Brunker, T. J.; Barlow, S.; O'Hare, D. *Chem. Commun.* **2001**, 2052−2053.
(4) Brunker, T. J.; Green, J. C.; O'Hare, D. *Inorg. Chem.* **2002**, *41*, 1701−1703.
(5) For some recent leading references, see the following: (a) Ruba, E.; Simanko, W.; Mereiter, K.; Schmid, R.; Kirchner, K. *Inorg. Chem.* **2000**, *39*, 382−384. (b) Tellers, D. M.; Bergman, R. G. *Organometallics* **2001**, *20*, 4819−4832. (c) Sanford, M. S.; Henling, L. M.; Grubbs, R. H. *Organometallics* **1998**, *17*, 5384−5389. (d) Gutierrez-Puebla, E.; Monge, A.; Paneque, M.; Poveda, M. L.; Taboada, S.; Trujillo, M.; Carmona, E. *J. Am. Chem. Soc.* **1999**, *121*, 346−354.
(6) Trofimenko, S. *Chem. Rev.* **1993**, *93*, 943−980.
(7) Jesson, J. P.; Trofimenko, S.; Eaton, D. R. *J. Am. Chem. Soc.* **1967**, *89*, 3148−3158.
(8) Sitzmann, H. *Coord. Chem. Rev.* **2001**, *214*, 287−327 and references therein.
(9) Warren, K. D. *Struct. Bonding (Berlin)* **1976**, *27*, 45−159 and references therein.
(10) Green, J. C. *Struct. Bonding (Berlin)* **1981**, *43*, 37−112.
(11) Long, N. J. *Metallocenes-an introduction to sandwich complexes*, 1st ed.; Blackwell Science Ltd.: Oxford, U.K., 1998.
(12) Jesson, J. P. *J. Chem. Phys.* **1966**, *45*, 1049−1056.
(13) Jesson, J. P. *J. Chem. Phys.* **1967**, *47*, 582−591.
(14) Jesson, J. P.; Trofimenko, S.; Eaton, D. R. *J. Am. Chem. Soc.* **1967**, *89*, 3158−3164.
(15) Jesson, J. P.; Weiher, J. F.; Trofimenko, S. *J. Chem. Phys.* **1968**, *48*, 2058−2066.
(16) Hutchison, B.; Daniels, L.; Henders, E.; Neill, P. *J. Chem. Soc., Chem. Commun.* **1979**, 1003−1004.
(17) Long, G. J.; Hutchinson, B. B. *Inorg. Chem.* **1987**, *26*, 608−613.
(18) Sohrin, Y.; Kokusen, H.; Matsui, M. *Inorg. Chem.* **1995**, *34*, 3928−3934.
(19) Bruno, G.; Centineo, G.; Cilberto, E.; Di Bella, S.; Fragala, I. *Inorg. Chem.* **1984**, *23*, 1832−1836.
(20) Janiak, C.; Scharmann, T. G.; Green, J. C.; Parkin, R. P. G.; Kolm, M. J.; Riedel, E.; Mickler, W.; Elguero, J.; Claramunt, R. M.; Sanz, D. *Chem.—Eur. J.* **1996**, *2*, 992−1000.
(21) Albright, T. A.; Burdett, J. K.; Whangbo, M. H. In *Orbital Interactions in Chemistry*; Wiley: New York, 1985.
(22) Troyanov, S. I.; Antropiusova, H.; Mach, K. *J. Organomet. Chem.* **1992**, *427*, 49−55.
(23) Cuenca, T.; Herrmann, W. A.; Ashworth, T. V. *Organometallics* **1986**, *5*, 2514−2516.
(24) Sanner, R. D.; Duggan, D. M.; McKenzie, T. C.; Marsh, R. E.; Bercaw, J. E. *J. Am. Chem. Soc.* **1976**, *98*, 8358−8365.
(25) Bercaw, J. E. *J. Am. Chem. Soc.* **1974**, *96*, 5087−5095.
(26) Hitchcock, P. B.; Kerton, F. M.; Lawless, G. A. *J. Am. Chem. Soc.* **1998**, *120*, 10264−10265.

Table 1. Solid-State Magnetic Susceptibility Data for Mixed-Sandwich Complexes with 14−19 Valence Electrons

complex	μ_{eff} (μ_B)[a]	Θ (K)[a]	temp range (K)
$[VCpTp]^+[BAr'_4]^-$	2.84	12.0	25−300
VCpTp	3.69	−1.8	20−300
$[CrCp^*Tp]^+[PF_6]^-$	3.75	−3.9	20−300
$CrCp^*Tp$	5.02	−0.4	10−300
$CoCp^*Tp$	1.85	−3.2	40−300
CoCpTp	5.8	*b*	300[b]
$[NiCp^*Tp]^+[PF_6]^-$	1.91	−9.1	10−300

[a] Values of μ_{eff} and Θ obtained from fitting to the Curie−Weiss law over the T range given. [b] Moment is strongly T dependent and does not follow Curie−Weiss behavior.

and $Ti\{C_5Me_4(SiMe_3)\}_2$ is reported to be paramagnetic, although no EPR signal was observed down to 77 K.[27] $[VCp^R_2]^+$ species are coordinatively unsaturated and tend to coordinate donor ligands; "naked" $[VCp_2]^+$ has recently been isolated, but no magnetic measurements were reported.[28] $[VTp_2]^+$ and $[VTp^*_2]^+$ are both reported to have moments of ca. 2.8 μ_B consistent with an $S = 1$ electronic ground state, but no EPR data have been reported for either.[29]

Solid-state magnetic susceptibility measurements performed on $[VCpTp]^+[BAr'_4]^-$ reveal essentially temperature-independent behavior between 25 and 300 K with a moment very close to the spin-only value for an $S = 1$ species (see Table 1). There is a reduction in the moment at low T (T = temperature) to 2.22 μ_B at 5 K, which may be a result of zero-field splitting effects, which are often observed for V(III) ions.[30]

We were able to obtain EPR spectra of $[VCpTp]^+[BAr'_4]^-$ at room temperature in CH_2Cl_2 and Et_2O solutions. In both cases two isotropic signals with hyperfine coupling to V (^{51}V, $I = 7/2$, 99.75% abundance) were observed with $g_1 = 1.991$ ($A_1 = 104.9 \times 10^{-4}$ cm^{-1}), $g_2 = 1.986$ ($A_2 = 66.2 \times 10^{-4}$ cm^{-1}) in Et_2O (300 K) and $g_1 = 1.994$ ($A_1 = 105.0 \times 10^{-4}$ cm^{-1}), $g_2 = 1.991$ ($A_2 = 65.1 \times 10^{-4}$ cm^{-1}) in CH_2Cl_2. At 4.5 K in CH_2Cl_2 solution, two components are resolved at $g \approx 2$ ($g_1 = 1.993$ ($A_1 = 70.4 \times 10^{-4}$ cm^{-1}), $g_2 = 1.949$ ($A_2 = 171.6 \times 10^{-4}$ cm^{-1})) as well as a broad feature at $g \approx 4.4$ which may be a double quantum transition. V(III), as a non-Kramer's ion, is usually EPR silent unless located in a site of high symmetry; reports of EPR spectra of such species are mainly restricted to studies on V(III) doped into various crystal lattices.[31,32] To our knowledge there is only a single report of EPR behavior in a molecular V(III) species, that of the tetrahedral ion $[V(C_6Cl_5)_4]^-$.[33] Thus there is little precedent to rationalize the spectra of $[VCpTp]^+$. The observation of two isotropic signals at room temperature is somewhat puzzling and implies that one may arise from an unidentified impurity; however neither signal corresponds to obvious impurities such as the reduced species VCpTp (vide infra) or adducts arising from the presence of adventitious quantities of σ-donor ligands.[34] Despite these complications, we conclude that the observation of an EPR signal at room T (and at low T) and the temperature-independent magnetic moment close to the spin-only value suggest an orbital singlet ground state. The ground state also appears to be different to the Ti(II) species detailed above, which are EPR silent and have magnetic moments somewhat less than the spin-only value. Two paramagnetic ground states are possible for a d^2 species according to the axially symmetric MO scheme, orbitally degenerate $\delta^1\sigma^1$ or orbitally nondegenerate δ^2. Although the magnetic data suggest the latter, crystallographic evidence and DFT calculations are consistent with the former (vide infra).

d^3 Species. The 15-electron metallocenes (VCp^R_2 and $[CrCp^R_2]^+$) adopt an orbitally nondegenerate $e_{2g}^2a_{1g}^1$ ($\delta^2\sigma^1$) electronic configuration: they therefore display temperature-independent moments close to the spin-only value for an $S = 3/2$ state (3.87 μ_B).[35−38] We have prepared two 15-electron species, VCpTp and $[Cp^*CrTp]^+[PF_6]^-$, both of which show temperature-independent moments over a wide range that are consistent with orbitally nondegenerate high-spin d^3 configurations (see Table 1). We see a substantial reduction in the moment of VCpTp below 20 K, to ca. 2.7 μ_B at 2 K which could arise as a consequence of intermolecular antiferromagnetism or a small zero-field splitting. (The zero-field splitting in VCp_2 has been investigated in some detail using EPR experiments at different magnetic fields.[39])

The 15-electron metallocenes also show simple EPR behavior associated with the orbitally nondegenerate $^4A_{2g}$ ground state. For VCp^R_2, isotropic spectra are often observed at room temperature in solution, as well as axially symmetric patterns in rigid media at low temperature.[39,40] There is little observed dependence of the hyperfine coupling constants on the diamagnetic host used in the experiment. EPR spectra for $[CrCp^R_2]^+$ species have not been observed at room temperature; however, in rigid media axially symmetric spectra have been observed. Hyperfine couplings are not resolved to ^{53}Cr ($I = 3/2$, 9.55% abundance) for $[CrCp_2]^+$[40] and $[Cr(C_5Ph_4H)_2]^+$,[38] whereas $[CrCp^*_2]^+$ displayed hyperfine coupling on $g_\perp$ only.[36] Some relevant data, including that for VCpTp and $[CrCp^*Tp]^+[PF_6]^-$, are summarized in Table 3. We recorded isotropic spectra of VCpTp at room temperature in toluene and Et_2O solution with almost identical g_{iso} and A_{iso} values in each case. In a frozen toluene

(27) Horacek, M.; Kupfer, V.; Thewalt, U.; Stepnicka, P.; Polasek, M.; Mach, K. *Organometallics* **1999**, *18*, 3572−3578.
(28) Calderazzo, F.; Ferri, I.; Pampaloni, G.; Englert, U. *Organometallics* **1999**, *18*, 2452−2458.
(29) Mohan, M.; Holmes, S. M.; Butcher, R. J.; Jasinski, J. P.; Carrano, C. J. *Inorg. Chem.* **1992**, *31*, 2029−2034.
(30) Carlin, R. L. *Magnetochemistry*; Springer-Verlag: Berlin, 1986.
(31) Schwartz, R. W.; Carlin, R. L. *J. Am. Chem. Soc.* **1970**, *92*, 6763−6771.
(32) Tregenna-Piggott, P. L. W.; Weihe, H.; Bendix, J.; Barra, A.-L.; Gudel, H.-U. *Inorg. Chem.* **1999**, *38*, 5928−5929.
(33) Alonso, P. J.; Fornies, J.; Garcia-Monforte, M. A.; Martin, A.; Menjon, B. *Chem. Commun.* **2001**, 2138−2139.
(34) The 16-electron species $[VCpTpL]^+$ (L = MeCN, ^{t}BuNC and PMe_3) are EPR silent at room temperature as powders and in solution but display powder EPR spectra below 10 K characterized by a very broad absorption at $g \approx 2$. There appears to be hyperfine coupling in all three cases, but it is poorly resolved.
(35) Leipfinger, H. *Z. Naturforsch., B: Anorg. Chem., Org. Chem.* **1958**, *13B*, 53−54.
(36) Robbins, J. L.; Edelstein, N.; Spencer, D.; Smart, J. C. *J. Am. Chem. Soc.* **1982**, *104*, 1882−1893.
(37) Fischer, E. O.; Ulm, K. *Chem. Ber.* **1962**, *95*, 692−694.
(38) Castellani, M. P.; Geib, S. J.; Rheingold, A. L.; Trogler, W. C. *Organometallics* **1987**, *6*, 1703−1712.
(39) Prins, R.; van Voorst, J. D. W. *J. Chem. Phys.* **1968**, *49*, 4665−4673.
(40) Ammeter, J. H. *J. Magn. Reson.* **1978**, *30*, 299−325.

Table 2. Magnetic Data for 20 Electron Species

compd	μ_{eff} (μ_B)	Θ (K)	temp range (K)	D (cm^{-1})[c]	$g_\perp$ [c]	ref
$NiCp_2$	2.89	6	70−300	25.6	2.06	66
$NiCp^*_2$	2.93	−15	6−100	30.5	1.74	36
$Ni(C_5Ph_4H)_2$	2.83	3	50−300	34.2	2.015	38
NiCp*Tp	2.93	−5.7	60−300	51.6	2.08	*b*
$NiTp_2$ [a]	3.22		300			7

[a] Magnetic moment measured by Evans' method in CD_2Cl_2. [b] This work. [c] Zero-field splitting parameter, D, and $g_\perp$ derived from $\chi = (2/3)N\mu_B^2[(g_{||}^2/kT)(e^{-D/kT}/(1 + 2e^{-D/kT})) + 2(g_\perp^2/D)((1 - e^{-D/kT})/(1 + 2e^{-D/kT}))]$ as described in text.

solution at 6.5 K an axially symmetric pattern is observed (a double quantum transition ($m_s = -3/2 \rightarrow +1/2$) is observed at $g \approx 4$, $g_\perp$, and the $m_s = -1/2 \rightarrow +1/2$ transition at $g \approx 2$, $g_{||}$) with coupling to V resolved on $g_\perp$ ($A_\perp = 54.6 \times 10^{-4}$ cm^{-1}). A complex pattern is observed for the $g_{||}$ component which could not be resolved. It is unclear as to whether, in addition to hyperfine coupling to V, there is extra splitting derived from coupling to protons on the Cp ring or to ^{14}N ($I = 1$, 99.63% abundance) or to both. A_{iso} and $A_\perp$ for VCpTp are substantially larger than those reported for VCp_2, which in turn are larger than those reported for VCp^*_2 and $V(C_5Ph_4H)_2$. We did not observe a room-temperature signal for $[CrCp^*Tp]^+[PF_6]^-$, but in a frozen MeCN solution at 14 K an axially symmetric pattern was obtained with no resolvable hyperfine coupling. A very similar spectrum was also obtained when attempting to record the spectrum of CrCp*Tp as a concentrated toluene solution: CrCp*Tp itself is found to be EPR silent using X-band (vide infra), but presumably an adventitious quantity of the oxidized species is present. (Both the spectra of $[CrCp_2]^+$ and $[CrCp^*_2]^+$ have been recorded due to the presence of adventitious impurities in samples obtained by cosublimation of the Cr(II) species with a diamagnetic host; the ease of oxidation of all these complexes explains these observations.[36,40]) It is worth noting that the lower symmetry of $[Cr(C_5Ph_4H)_2]^+$ with respect to $[CrCp_2]^+$ and $[CrCp^*_2]^+$ causes the assumption of axial symmetry to break down, hence the resolution of both g_x and g_y components at apparent $g \approx 4$.[38] This splitting is not observed for isoelectronic $V(C_5Ph_4H)_2$ perhaps since this spectrum is further complicated by hyperfine coupling to V. Thus magnetic and EPR data observed for VCpTp and $[CrCp^*Tp]^+$ are very similar to that for the corresponding metallocene species and are thus consistent with an orbitally nondegenerate ground state, hence a $\delta^2\sigma^1$ configuration.

d^4 Species. The 16-electron metallocenes $CrCp_2$, $CrCp^*_2$, and $[MnCp^*_2]^+[PF_6]^-$ adopt an orbitally degenerate spin-triplet state ($^3E_{2g}$ or $^3\Delta$) arising from a $\delta^3\sigma^1$ electronic configuration.[36,41,42] This is in agreement with the predictions of the metallocene MO scheme in which there is a small energy separation between the weakly bonding/nonbonding δ- and σ-levels and the strongly antibonding π-orbitals. The reported moments are consistent with an $S = 1$ state (spin-only moment is 2.83 μ_B) with some orbital contribution, and such species are found to be EPR silent (with X-band) due to efficient relaxation processes of the spin triplet ground state. High-spin ($S = 2$) states have been enforced in chromocenes by use of extremely bulky ring substituents (1,2,3,4,1′,2′,3′,4′-octaisopropylchromocene undergoes a gradual spin-transition from a moment of 2.83 μ_B at 2 K to 4.90 μ_B at 300 K),[43] and in certain substituted bis(indenyl)-chromium(II) complexes.[44] No EPR behavior has been reported for $S = 2$ d^4 metallocenes.

The 16-electron complex CrCp*Tp was found to obey the Curie−Weiss law over the range 10−300 K, with a moment of 5.02 μ_B at 300 K ($\Theta = -0.4$ K). This is slightly greater than the spin-only value for 4 unpaired electrons (4.89 μ_B) and is indicative of a high-spin $\delta^2\sigma^1\pi^1$ configuration. The high-spin d^4 configuration is susceptible to Jahn−Teller distortion, as is observed in the crystal structure of CrCp*Tp (vide infra). Jahn−Teller distortion should lead to a partial quenching of the orbital contributions to the moment, but in this case the resultant moment is still slightly greater than the spin-only value. $CrTp_2$ also displays a moment consistent with 4 unpaired electrons,[45] as does a substituted analogue.[46] We did not observe an EPR signal for CrCp*Tp at room temperature or below 20 K in toluene solution. In a concentrated sample a signal was observed that was attributed to the fortuitous presence of some of the oxidized species (vide supra). $S = 2$ Cr(II) species are often EPR silent using X-band although recently such species have been probed by use of high-field EPR experiments.[47]

d^6 Species. The 18-electron metallocene species (including $[MnCp^*_2]^-$, $FeCp^R_2$, $[CoCp^R_2]^+$, and $[NiCp^*_2]^{2+}$) are without exception diamagnetic.[8,36,42] In our studies we synthesized five 18-electron complexes FeCp*Tp, $[FeCp^*Tpm]^+[PF_6]^-$, $[CoCp^*Tp]^+[PF_6]^-$, $[CoCpTp]^+[X]^-$, and $[CoCpTpm]^{2+}[X]_2^-$ (in the case where $X = PF_6^-$ or I^-, the counterion has no effect on the properties of the cation as indicated by identical solution NMR and UV/vis spectra). All these species are diamagnetic in solution at room temperature, with the notable exception of FeCp*Tp which is characterized by a typical paramagnetically broadened and shifted ^1H NMR spectrum in all solvents studied at room temperature;[2] the solution magnetic moment of FeCp*Tp was determined in C_6D_6 solution by the Evans NMR method and was found to be 2.0 μ_B at 291 K. SQUID magnetometry on solid samples of FeCp*Tp at 300 K displayed no signal, but on heating above 300 K a paramagnetic signal was observed; however, the decomposition of FeCp*Tp at elevated temperatures precluded data collection. We conclude that FeCp*Tp is diamagnetic or almost diamagnetic at 300 K in the solid state (with any weak paramagnetism canceled out by the inherent diamagnetism associated with the closed-shell electrons to

(41) Engelmann, F. *Z. Naturforsch., B: Anorg. Chem., Org. Chem.* **1953**, *8B*, 775−776.
(42) Robbins, J. L.; Edelstein, N. M.; Cooper, S. R.; Smart, J. C. *J. Am. Chem. Soc.* **1979**, *101*, 3853−3857.
(43) Sitzmann, H.; Schar, M.; Dormann, E.; Kelemen, M. *Z. Anorg. Allg. Chem.* **1997**, *623*, 1850−1852.
(44) Brady, E. D.; Overby, J. S.; Meredith, M. B.; Mussman, A. B.; Cohn, M. A.; Hanusa, T. P.; Yee, G. T.; Pink, M. *J. Am. Chem. Soc.* **2002**, *124*, 9556−9566.
(45) Dapporto, P.; Mani, F.; Mealli, C. *Inorg. Chem.* **1978**, *17*, 1323−1329.
(46) Brunker, T. J.; Hascall, T.; Cowley, A. R.; Rees, L. H.; O'Hare, D. *Inorg. Chem.* **2001**, *40*, 3170−3176.
(47) Telser, J.; Pardi, L. A.; Krzystek, J.; Brunel, L.-C. *Inorg. Chem.* **1998**, *37*, 5769−5775.

Table 3. EPR Data for 15-Electron Complexes

complex	host	T (K)	$g_\perp$ [a]	$g_\parallel$	$A_\perp$ [b]	$A_\parallel$ [b]	ref
VCpTp	toluene	304	$g_{iso} = 1.993$		$A_{iso} = 59.2$		*c*
	Et_2O	298	$g_{iso} = 1.992$		$A_{iso} = 59.8$		*c*
	toluene	7	1.995	d	54.6	d	*c*
VCp_2	$FeCp'_2$ [e]	300	$g_{iso} = 2.003$		$A_{iso} = 25.4$		40
	$FeCp_2$	4	1.988	1.999	21.0	35.7	40
VCp^*_2	toluene	300	$g_{iso} = 1.985$		$A_{iso} = 23.1$		36
	$MgCp^*_2$	24	1.996	2.005	17.1	31.8	36
$[CrCp^*Tp]^+$ [f]	MeCN	14	2.062	2.06			*c*
$[CrCp^*Tp]^+$ [g]	toluene	18	1.98	1.996			*c*
$[CrCp_2]^+$ [f]	$MgCp_2$	4	1.977	2.002			40
$[CrCp^*_2]^+$ [f]	$[CoCp_2]^+$ [f]	17	2.01	2.001	253		36

[a] Double quantum transition; observed g is twice that quoted. [b] Units 10^{-4} cm^{-1}. [c] This work. [d] Values could not be resolved. [e] Cp′ = methylcyclopentadienyl. [f] $[PF_6]^-$ salt. [g] Sample was a solution of CrCp*Tp in toluene; see main text.

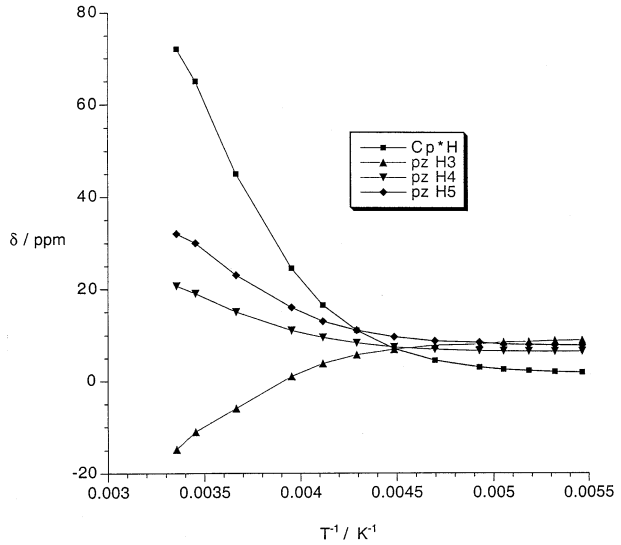

Figure 3. Variation of δ (ppm) with T^{-1} (K^{-1}) for ^1H NMR resonances ([D_8]toluene) of FeCp*Tp. The labels for the pyrazolyl protons are in accordance with the nomenclature for Tp ligands outlined in ref 6.

give no measurable signal) but in solution exists in a spin equilibrium between low-spin $S = 0$ and high-spin $S = 2$ forms (high-spin Fe^{II}, $S = 2$, spin-only moment 4.89 μ_B; low-spin Fe^{II}, $S = 0$).

To confirm this hypothesis we conducted a series of variable-temperature solution ^1H NMR experiments. For a simple molecular paramagnet the temperature dependence of the chemical shifts should follow the Curie Law;[48] however in this case we observed a marked nonlinear dependence of δ with $1/T$ (as shown in Figure 3). At 180 K, the observed chemical shifts were very similar to those observed for $[FeCp^*Tpm]^+$ and another isoelectronic diamagnetic species $[CoCp^*Tp]^+$. This behavior was similar in all solvents investigated and can be visually followed as on cooling solutions show a pronounced color change form green/blue to sky blue. Qualitatively these observations suggest an $S = 0$ ground state, with a thermally accessible $S = 2$ state; similar spin-equilibrium behavior has previously been successfully modeled as a simple Boltzmann distribution of spins for various Co(III) complexes[49,50] and in probing the electronic structure of NiCp*(acac).[51] The temperature dependence of the chemical shifts is related to the thermodynamic parameters by

$$\delta = \delta_{LS} + \frac{C}{T[1 + e^{(\Delta H - T\Delta S)/RT}]} \quad (1)$$

where δ is the observed chemical shift, δ_{LS} is the calculated shift for the diamagnetic species, C is a constant related to the molar susceptibility of the HS species, and ΔH and ΔS are the enthalpy and entropy changes associated with the spin transition.

We performed a similar analysis for the temperature dependence of the ^1H NMR chemical shifts for FeCp*Tp. Fitting was performed on data obtained in two solvents of different polarity, [D_8]THF and [D_8]toluene, using δ (Cp*H) only as the Tp resonances overlapped at many of the temperatures, making accurate determination of δ difficult. δ_{LS} was set as the value observed for $[CoCp^*Tp]^+$. A plot of the actual and fitted data is shown in Figure 4, and the calculated thermodynamic terms are given in Table 4. In both cases the values of ΔH and ΔS are positive in agreement with all other observations of spin transitions.[52] ΔH is positive is due to weakening of the metal−ligand bonding in the HS state due to occupancy of antibonding π-orbitals. ΔS is positive as a result of several factors including an increase in electronic degeneracy and in vibrational and rotational degrees of freedom in the HS form. It lies well within the range measured for various Fe(II) complexes in solution (ca. 33−110 J mol^{-1} K^{-1}).[53,54] There is a slight solvent effect in the entropic contribution also: presumably the solvation of the molecule varies with the spin state, and there is an entropy change associated with the difference in solvation between the two forms, the magnitude of which depends on the solvent.

The calculated equilibrium constant, K, in [D_8]toluene, is 0.34 at 291 K, where K = [% HS]/[% LS]; hence, assuming

(48) Horrocks, W. D., Jr. In *NMR of Paramagnetic Molecules*; LaMar, G. N., Horrocks, W. D., Jr., Holm, R. H., Eds.; Academic Press: New York, 1973.

(49) Gutlich, P.; McGarvey, B. R.; Klaui, W. *Inorg. Chem.* **1980**, *19*, 3704−3706.

(50) Klaui, W.; Eberspach, W.; Gutlich, P. *Inorg. Chem.* **1987**, *26*, 3977−3982.

(51) Smith, M. E.; Andersen, R. A. *J. Am. Chem. Soc.* **1996**, *118*, 11119−11128.

(52) Gutlich, P.; Hauser, A.; Spiering, H. *Angew. Chem., Int. Ed. Engl.* **1994**, *33*, 2024−2054.

(53) Dose, E.; Hoselton, M. A.; Sutin, N.; Tweedle, M. F.; Wilson, L. J. *J. Am. Chem. Soc.* **1978**, *100*, 1141.

(54) Reeder, K. A.; Dose, E. V.; Wilson, L. J. *Inorg. Chem.* **1978**, *17*, 1071.

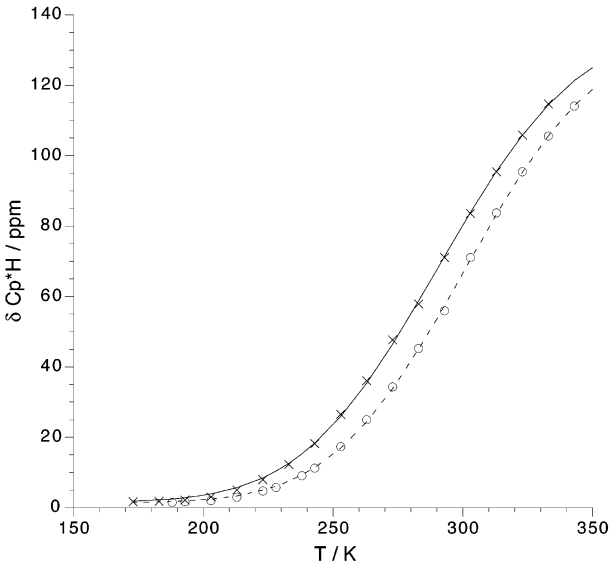

Figure 4. Plot of experimental (×, [D_8]THF; ○ [D_8]toluene) and calculated (— [D_8]THF, ---, [D_8]toluene) ^{1}H NMR Cp*H resonances for FeCp*Tp against *T*.

Table 4. Parameters for the LS ⇔ HS Equilibrium of FeCp*Tp in toluene-d_8 and THF-d_8 Solution, Obtained from Fitting ^{1}H NMR Data to Eq 1

solvent	C	ΔH (kJ/mol)	ΔS (J/(mol K))
THF-d_8	62 140	+23.1	+72.8
toluene-d_8	60 870	+25.9	+80.1

spin-only behavior for the $S = 2$ form, a value of 2.5 μ_B is calculated for the moment at 291 K. This is in good agreement with Evans' method moment at this temperature, confirming the interpretation of the solution behavior.

This behavior is in fact very similar to the case of $FeTp_2$, which is diamagnetic at room temperature in the solid state but undergoes a spin transition at elevated temperaures.[16] In solution it displays a moment of 2.71 μ_B at room temperature, indicating a spin-equilibrium species, and the ^{1}H NMR chemical shifts tend to diamagnetic values at low T also rather than displaying Curie-like behavior.[14,55] The spin states of substituted bis(Tp)iron(II) complexes are very sensitive to substituents on the pyrazolyl rings and on B.[18] The difference in behavior between FeCp*Tp and [FeCp*Tpm]$^+$-[PF_6]$^-$ in solution again emphasizes the subtle factors that determine spin state in these and related complexes.

d^7 Species. The 19-electron metallocenes exhibit temperature-dependent magnetic moments consistent with a single unpaired electron but deviate significantly from the spin-only value (1.73 μ_B) for an $S = 1/2$ state.[36,38,56,57] These observations are consistent with an orbitally degenerate $^2E_{1g}$ ($^2\Pi$) ground state arising from the electronic configuration $e_{2g}^4\ a_{1g}^2\ e_{1g}^1$ ($\delta^4\sigma^2\pi^1$) predicted on the basis of the metallocene MO scheme. The theory underpinning the experimental EPR observations for 19-electron $^2E_{1g}$ metallocenes is complex and has been extensively studied.[40,58−60] Signals are observed only at very low temperatures (4 K), due to the short relaxation times associated with the degenerate ground state. The *g* and *A* values display marked host and substituent dependence as the degenerate ground state is susceptible to distortions imposed externally by the lattice or internally from Jahn−Teller distortions. The *g* tensors observed are rhombic (i.e. $g_x \neq g_y \neq g_z$) generally with hyperfine coupling on all three components (^{59}Co, $I = 7/2$, 100% abundant; ^{61}Ni, $I = 3/2$, 1.1% abundant and only observed if the complex is isotopically enriched).

We have synthesized four metal sandwich complexes CoCp*Tp, CoCpTp, [CoCpTpm]$^+$[PF_6]$^-$, and [NiCp*Tp]$^+$-[PF_6]$^-$ which are nominally 19-electron complexes. We have previously reported that in its crystal structure CoCp*Tp displays a 2-coordinate Tp ligand and should therefore be regarded as a 17-electron complex (with the Tp ligand acting as a 4-electron donor). Evidence from IR spectroscopy indicates that in solution a 3-coordinate Tp structure is also adopted, however, indicating a structural equilibrium between the 17 and 19 electron species. Solid-state magnetic susceptibility data for CoCp*Tp can be fitted to the Curie−Weiss law over the temperature range 40−300 K giving a moment of 1.85 μ_B; however, at low-temperature we observe a decrease in the moment to 1.18 μ_B at 5 K. We have measured the moment in solution by the Evans NMR method to be 2.5 μ_B (in C_6D_6), consistent with a single unpaired electron with a large orbital contribution. No EPR signal was observed in toluene solution at room temperature; however in a frozen solution at 15 K, a rhombic spectrum was observed with hyperfine coupling to ^{59}Co ($I = 7/2$) resolved on all three components (for values see Table 5). The magnetic data are thus in agreement for a species with a single unpaired electron over the entire temperature range. The data can be interpreted in a fashion similar to the analogous compound CoCp*(acac) which has a ^{2}A ground state (arising from occupancy of a single π-orbital)[51] and in which the solid-state magnetic and low-temperature EPR data indicate that the orbital angular momentum is not completely quenched. Smith and Andersen observe an EPR spectrum at room temperature also: presumably in our case the conformational exchange in solution provides an efficient relaxation pathway and thus no signal is observed.

In contrast CoCpTp is a true 19-electron complex, with 3-coordinate Tp ligation indicated from the crystal structure and from IR data. In the solid state CoCpTp does not obey the Curie−Weiss Law and displays distinctly temperature-dependent behavior. A room-temperature moment of 5.80 μ_B is observed, and the moment increases to a maximum of ca. 6.9 μ_B at 50 K, before decreasing to ca. 6.2 μ_B at 5 K. Clearly, this is inconsistent with a single unpaired electron but is more reasonable for a high-spin d^7 or $S = 3/2$ ground state with a large orbital contribution (spin-only value is 3.89

(55) Holm, R. H.; Hawkins, C. J. In *NMR of Paramagnetic Molecules*; LaMar, G. N., Horrocks, W. D., Jr., Holm, R. H., Eds.; Academic Press: New York, 1973.
(56) Gordon, K. R.; Warren, K. D. *Inorg. Chem.* **1978**, *17*, 987−994.
(57) Burkey, D. J.; Hays, M. L.; Duderstadt, R. E.; Hanusa, T. P. *Organometallics* **1997**, *16*, 1465−1475.
(58) Ammeter, J. H.; Swalen, J. D. *J. Chem. Phys.* **1972**, *57*, 678−698.
(59) Ammeter, J. H.; Oswald, N.; Bucher, R. *Helv. Chim. Acta* **1975**, *58*, 671−682.
(60) Rajasekharan, M. V.; Bucher, R.; Deiss, D.; Zoller, L.; Salzer, A. K.; Moser, E.; Weber, J.; Ammeter, J. H. *J. Am. Chem. Soc.* **1983**, *105*, 7516−7522.

Table 5. EPR Data for d^7 Complexes

complex	T (K)	g_x	g_y	g_z	A_x[a]	A_y[a]	A_z[a]	ref
CoCp*Tp[d]	14	1.971[c]	2.086[c]	2.177[c]	32[c]	22[c]	84[c]	*b*
CoCp*(acac)[e]	300		$g_{iso} = 2.099$			$A_{iso} = 44.3$		51
	2	1.970[c]	2.091[c]	2.241[c]	39.6[c]	small	110.3[c]	51
[NiCp*Tp]$^+$ [f,g]	11	2.095[h]	2.142[h]	2.037[h]				*b*
$CoCp^*_2$ [i]	9	1.693	1.733	1.754	<6	111	65	36
$CoCp_2$ [j]	4	1.755	1.847	1.693		173	90	58
$[NiCp^*_2]^+$ [f,k]	8	1.973	2.014	1.831				36
$[NiCp^*_2]^+$ [f,l]	4	1.973	2.016	1.801	0[m]	47.5[m]	16[m]	60

[a] Units 10^{-4} cm^{-1}. [b] This work. [c] Axes not assigned. [d] Toluene solution. [e] Methylcyclohexane solution. [f] $[PF_6]^-$ salt. [g] Powdered sample. [h] Assignment of axes uncertain but follows convention that for $[NiCp_2]^+$ generally $g_y > g_x > g_z$. [i] $FeCp^*_2$ host. [j] $FeCp_2$ host. [k] $[CoCp^*_2]^+[PF_6]^-$ host. [l] $[CoCp_2]^+[PF_6]^-$ host. [m] *A* values derived from sample enriched in ^{61}Ni.

μ_B). High-spin octahedral Co(II) complexes typically display room-temperature moments in the range 4.7−5.4 μ_B,[61] and considerable temperature dependence of the moments in such species is also expected, due to thermal occupancy of energy levels arising from spin−orbit coupling. No EPR signal was observed for CoCpTp either in toluene solution at room temperature or at low temperature in a toluene glass. EPR signals are often observed for high-spin Co(II) (vide infra) species in a variety of coordination geometries, although usually only at liquid-He temperatures as excited states close in energy to the ground state generally provide efficient relaxation of the electron spin.[61] Presumably the electronic relaxation is very efficient for CoCpTp, and so no signal is observed. CoCpTp is the first example of an organometallic cobalt complex which adopts a maximum spin configuration in preference to a potential low-spin alternative; i.e., there is preferential occupancy of an antibonding d-orbital over a vacant nonbonding or bonding level.[8] All known monomeric and dimeric Cp^RCo^{II} half-sandwich complexes and cobaltocenes are low-spin $S = 1/2$ complexes.[51,62]

In many ways, CoCp*Tp and CoCpTp show behavior analogous to that of classical coordination complexes. Low-spin octahedral complexes of Co(II) are very uncommon—the $t_{2g}^6e_g^1$ configuration is susceptible to Jahn−Teller distortion, and such species tend to lose a ligand(s) and form low-spin 4- or 5-coordinate species.[63] The flexibility of the Tp ligand thus allows the formation of a lower coordinate complex in the low-spin form. By comparison, structurally characterized cobaltocenes show no evidence of structural distortion despite the Jahn−Teller instability of the $^2E_{1g}$ ground state.[57,64,65] The rigidity of the cyclic Cp ligand presumably prohibits any gross deviations from axial symmetry, although there is crystallographic evidence for a subtle static distortion in $MnCp^*_2$ (ground state $^2E_{2g}$).[42] Detailed studies of the electronic structure of cobaltocenes through EPR measurements indicate that a dynamic Jahn−Teller distortion mechanism predominates over static distortions and leads to the observed *g* anisotropy.[40]

The spin state of $[CoCpTpm]^+[PF_6]^-$ is of interest as the molecule is a cationic analogue of CoCpTp and the ligand-field strengths of Tp and Tpm are expected to be very similar (vide infra). Unfortunately problems associated with the purification and instability of the complex precluded the collection of solid-state and solution magnetic moment data. The form of the solution NMR spectrum is however notably similar to that of CoCpTp suggesting it is high spin in solution (this may explain the lability of the complex also and its tendency to decompose to $[CoCp_2]^+$).[2] We were able to obtain EPR data in situ by reduction of $[CoCpTpm]^{2+}$ with less than 1 equiv of $CoCp_2$ in THF, generating three species in solution two of which ($[CoCpTpm]^{2+}$ and $[CoCp_2]^+$) are diamagnetic and thus EPR silent. At room temperature this solution gave no EPR signal; however, on cooling to 95 K a broad isotropic signal was observed, characterized by $g_{iso} = 2.06$. (The broadness may be attributable to intermolecular electronic exchange between mono- and dicationic species.) Further cooling to 6 K give an increase in resolution, and a complex signal was observed consistent with an anisotropic *g*-tensor with hyperfine coupling both to N and Co. Although little quantitative data were extracted from these observations, the form of these low-temperature spectra is consistent with a species with a LS $^2\Pi$ ground state. $CoTp_2$ and $[CoTpm_2]^{2+}$ (which are both HS) have been extensively studied by single-crystal and powder EPR studies.[12] The lowest Kramer's doublet arising from spin−orbit coupling of the $S = 3/2$ ground state in $CoTp_2$ has been characterized by the *g* values $g_{||} = 8.46$ and $g_\perp = 0.98$ (with hyperfine coupling to Co of 364×10^{-4} cm^{-1}); similar values were observed for $[CoTpm_2]^{2+}$. The data for $[CoCpTpm]^+$ are clearly inconsistent therefore with that observed for the analogous HS species. We tentatively conclude that $[CoCpTpm]^+$ may display spin-crossover behavior, although more high-temperature evidence of the HS state is required to confirm this proposition. It is likely however that variation of the substituents on the Tp ligand could affect the spin state in such systems.

$[NiCp^*Tp]^+[PF_6]^-$ obeys the Curie−Weiss law between 10 and 300 K with a moment somewhat greater than the spin-only moment for a single unpaired electron. In powdered samples, EPR signals were not observed at room temperature

(61) Banci, L.; Bencini, A.; Benelli, C.; Gatteschi, D.; Zanchini, C. *Struct. Bonding (Berlin)* **1982**, *52*, 37−86.
(62) Koelle, U.; Fuss, B.; Belting, M.; Raabe, E. *Organometallics* **1986**, *5*, 980−987.
(63) Cotton, F. A.; Wilkinson, G. *Advanced Inorganic Chemistry*, 5th ed.; Wiley-Interscience: New York, 1988.
(64) Bunder, W.; Weiss, E. *J. Organomet. Chem.* **1975**, *92*, 65−68.
(65) There is mention of an observable static distortion in the room-temperature crystal structure of $CoCp^*_2$ (see ref 36 of the following: Robbins, J. L.; Edelstein, N.; Spencer, D.; Smart, J. C. *J. Am. Chem. Soc.* **1982**, *104*, 1882−1893); however, to the best of our knowledge this structure has never been reported. In general, static Jahn−Teller effects in such complexes are very subtle and are likely only to be detected in very high quality crystal structures.

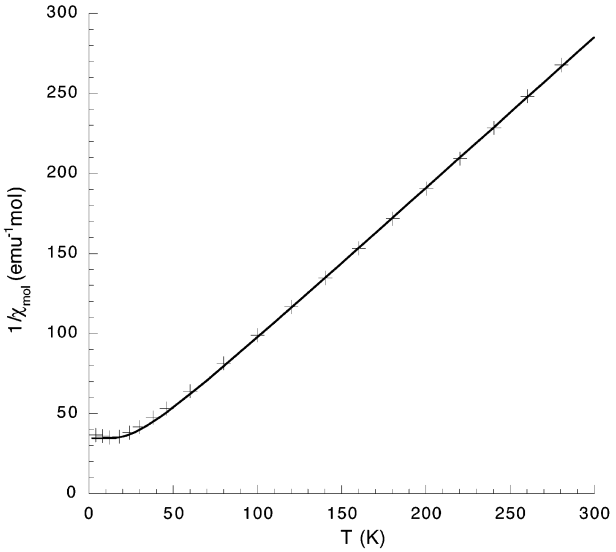

Figure 5. Plot of calculated (—) and experimental (+) values of $1/\chi_{mol}$ vs T for NiCp*Tp.

although at 11 K a rhombic spectrum was observed with the g-values close to 2 (see Table 5), consistent with a $^2\Pi$ ground state. Although we have no crystallographic evidence for the structure of $[NiCp^*Tp]^+[PF_6]^-$, IR data indicate a 3-coordinate Tp structure at room temperature in the solid-state. The ground state of $[NiCp^*Tp]^+[PF_6]^-$ therefore appears to be orbitally degenerate and similar to that of other 19-electron metallocenes.

d^8 Species. The magnetic moments of $NiCp^R_2$ complexes obey the Curie−Weiss law at high temperature and are close to the spin-only value; hence, an orbitally nondegenerate $^3A_{2g}$ $[e_{2g}{}^4a_{1g}{}^2e_{1g}{}^2]$ ground-state formulation is proposed.[36,38,66] For all $NiCp^R_2$ species studied the magnetic susceptibility curve becomes essentially independent of temperature below ~70 K. Prins et al. attributed this effect in $NiCp_2$ to a large zero-field splitting (ZFS) of the otherwise orbitally nondegenerate ground state.[66] The ZFS parameter, D, has been calculated in such systems and is reported, along with other magnetic data, in Table 2. EPR signals are not observed using X-band either at room temperature or at low temperature as the large value of D shifts the relevant transitions out of the energy range of the microwaves utilized for the experiment. $NiTp_2$ has a moment of 3.22 μ_B at room temperature,[7] consistent with a *pseudo*octahedral species with a small orbital contribution; however, no variable-temperature susceptibility studies have been performed.

The magnetic behavior of NiCp*Tp is similar to that for nickelocene species: it obeys the Curie−Weiss law above 60 K with a moment (2.93 μ_B) close to the spin-only value for an $S = 1$ complex (2.83 μ_B), but below ca. 30 K, $1/\chi_M$ becomes essentially independent of temperature.[67] We assume a large ZFS of a nondegenerate triplet ground state is also responsible for this behavior and for the absence of an EPR signal for NiCp*Tp either at 298 K or below 20 K. We thus followed the method of Prins et al. for calculating the ZFS parameter.[66] The magnetic susceptibility data is in good agreement with a model assuming the free-electron value for $g_{||}$ and values of $g_\perp = 2.08$ and $D = 51.6$ cm^{-1}, and a plot of the actual and fitted data is given in Figure 5. Comparison of these parameters with other $NiCp^R_2$ species shows that the value of $g_\perp$ is in good agreement and D is somewhat larger than those previously calculated. The large value of D for $NiCp_2$ was interpreted by Prins to indicate that the MO's containing the unpaired electrons have substantial metal character which is consistent with the $e_{2g}{}^4a_{1g}{}^2e_{1g}{}^2$ configuration. Our results therefore suggest a higher degree of metal character in the orbitals of π symmetry with respect to the principal axis in NiCp*Tp than in the e_{1g} set in nickelocenes.

In summary, the magnetic data indicate that the complexes of d^3, d^6, and d^8 configurations are similar electronically to the metallocene analogues, except for FeCp*Tp which displays a spin equilibrium in solution. These cases are the most simple requiring half-filling (d^3) and filling (d^6 and d^8) the σ and δ manifolds, although in the case of Fe(II) we can readily see that the energy gap to the higher energy π-levels is now comparable to the spin-pairing energy. In the d^4 and d^7 cases, we observe the high-spin state adopted for Cr(II) and Co(II), although the greater ligand-field strength associated with Cp* as opposed to Cp favors the low-spin configuration for CoCp*Tp. $[VCpTp]^+$ is paramagnetic and behaves as an orbitally nondegenerate species.

Optical Spectra of Mixed-Sandwich Complexes, MCp^RTp. The optical spectra of axially symmetric metallocenes have provided much useful information regarding the splitting of the frontier MO's (from d−d transitions) and the location of filled and empty ligand-based levels (from charge-transfer transitions).[9] With respect to d−d spectra, three cases emerge where theory predicts a simple spectrum consisting of three spin-allowed d−d bands: d^3, d^6 (low-spin), and d^8 configurations. In these situations straightforward analysis is possible and expressions have been derived that allow the calculation of the ligand-field splitting parameters Δ_1, Δ_2, and B (and C), which have been utilized in several studies of these metallocene species. For neutral metallocene species, bands assigned as spin-allowed d−d transitions typically have extinction coefficients (ϵ) in the range 10^1−10^2, whereas for cationic metallocene species they are usually 1 order of magnitude greater being in the range 10^2−10^3. The optical spectra of MTp_2 complexes with these same electronic configurations have also been studied and ligand-field parameters derived.

We have studied the electronic spectra of some MCp^RTp species assuming an axially symmetric ligand-field scheme. DFT calculations (vide infra) show that, for orbitally nondegenerate MCp^RTp species, the secondary splitting of the near-degenerate π- and δ-levels (due to the lower than pure axial symmetry) can be ignored to a first approximation. These calculated splittings are typically much smaller than

(66) Prins, R.; van Voorst, J. D. W.; Schinkel, C. J. *Chem. Phys. Lett.* **1967**, *1*, 54−55.

(67) A slight upturn in the χ_M vs T curve at 4 K can be attributed to a very small amount of an unidentified paramagnetic impurity: In two independently prepared samples the degree of this upturn was slightly different (although both samples analyzed correctly for NiCp*Tp); however, the other features of the χ_M curve remained the same.

Table 6. Ligand-field Absorption Data and Parameters for 15-Electron Metallocenes and Related Species[a]

	$^4A_{2g} \rightarrow {}^4E_{1g}(a)$; $^4\Sigma \rightarrow 4\Pi(a)$	$^4A_{2g} \rightarrow {}^4E_{2g}$; $^4\Sigma \rightarrow {}^4\Phi$	$^4A_{2g} \rightarrow {}^4E_{1g}(b)$; $^4\Sigma \rightarrow {}^4\Pi(b)$	Δ_1	Δ_2	B	β[f]
VCp_2 [b]	17 330 (58)	20 240 (46)	24 500 (66)	4930	16 420	420	0.55
VCp^*_2 [c]	18 700 (23)	20 600 (25)	28 200 (1037)	3800	18 700	630	0.82
VCpTp[d]	15 400 (75)	23 000[g]	27 000 (1700)	10700	13 700	270	0.35
		25 000		11700	14 100	470	0.61
$[CrCp_2]^+$ [e]	17 860 (270)	21 980 (210)	27 030 (630)	6760	16 570	510	0.55
$[CrCp^*_2]^+$ [c]	20 400 (1386)	23 100 (2450)	29 000[h]	4900	19 800	540	0.58
			32 000	5200	20 200	760	0.82
$[Cp^*CrTp]^+$ [d]	19 300 (1100)	25 900 (880)	29 500 (1350)	9350	17 820	420	0.46

[a] Transitions between states are given in D_{5d} and $C_{\infty v}$ notations. Energies in cm^{-1}. Extinction coefficients (mol^{-1} dm^3 cm^{-1}) are given in parentheses. [c] Data from ref 86. [c] Data from ref 36. [d] This work. [e] Data from ref 37. [f] Nephelauxetic ratio given by $B_{complex}/B_{free\ ion}$, where $B_{complex}$ is value listed and $B_{free\ ion}$ is the value in the gaseous transition metal ion as listed in ref 87. [g] This transition is partially obscured by another d−d band; thus the energies given are the estimated minimum and maximum values. [g] This transition is masked by a charge-transfer band; thus the energies given are the estimated minimum and maximum values.

Table 7. UV/Vis Data for 18-Electron Species, Spin-Allowed Bands, and Calculated Ligand-Field Parameters[a]

	$^1A_{1g} \rightarrow {}^1E_{1g}(a)$; $^1\Sigma \rightarrow {}^1\Pi(a)$	$^1A_{1g} \rightarrow {}^1E_{2g}$; $^1\Sigma \rightarrow {}^1\Phi$	$^1A_{1g} \rightarrow {}^1E_{1g}(b)$; $^1\Sigma \rightarrow {}^1\Pi(b)$	Δ_1	Δ_2	B	β[e]
$FeCp_2$ [b]	21 800 (36)	24 000 (72)	30 800 (49)	7100	22 000	390	0.39
$FeCp^*_2$ [c]	23 500 (121)	30 500 (180)	34 500 (2970)	11 200	23 100	420	0.40
$[CoCp_2]^+$ [b]	24 300 (140)	26 400 (120)	33 300 (1200)	7200	24 400	400	0.36
$[CoCp^*_2]^+$ [c]	23 800 (330)	29 500 (1430)	40 000 (1170)	14 100	24 100	630	0.57
$[CoCp^*Tp]^+$ [d]	17 500 (730)	24 500 (150)	30 300 (800)	12 670	16 800	380	0.35
$[CoCpTp]^+$ [d]	18 450 (850)	27 000 (200)	31 000 (640)	12870	17 780	280	0.25
$[CoCpTpm]^{2+}$ [d]	19 050 (830)	27 000 (300)	32 000−33 000 (900−1100)[g]	13 940−13 150	18 250−18 270	400−340	0.37−0.31
$FeCp^*Tp$[d]	16 500 (65)	24 000 (175)	26 000−30 000 (<2000)[g]	9940−13 410	15 990− 15 750	150−400	0.14−0.38

[a] All energies are in cm^{-1}; extinction coefficients are in mol^{-1} dm^3 cm^{-1} and are given in parentheses. [b] Data from ref 68. [c] Data from ref 36. [d] This work. [e] Nephelauxetic ratio given by $B_{complex}/B_{free\ ion}$, where $B_{complex}$ is value listed and $B_{free\ ion}$ is the value in the gaseous transition metal ion as listed in ref 87. [g] Estimated minimum and maximum values for band.

the bandwidths observed in the experimental spectra and so would not be resolved.

d^3 Species. The three one-electron spin-allowed transitions from the $^4A_{2g}$ ground state of a d^3 metallocene yield the excited states $^4E_{1g}(a)$, $^4E_{2g}$, $^4E_{1g}(b)$;[9] Prins and van Voorst have given expressions that relate the energy of these transitions with the parameters Δ_1, Δ_2, and B.[39] (In addition five spin-forbidden transitions are predicted to occur at lower energy; however, these will not be considered further here.) Thus, correct assignment of the bands allows calculation of these three parameters. For the metallocene species the energy ordering of the excited states was found to be $^4E_{1g}(b) > {}^4E_{2g} > {}^4E_{1g}(a)$; this implies that the a_{1g} (σ) level lies above the e_{2g} (δ) level in energy. Incorrect assignments give imaginary values of B and can thus be rejected. Table 6 lists the spin-allowed transitions observed and the derived ligand-field parameters for some 15-electron metallocene species and the mixed-sandwich species VCpTp and $[CrCp^*Tp]^+[PF_6]^-$. Symmetry labels are given also in $C_{\infty v}$ symmetry for completeness.

The spectrum of VCpTp shows only two well-resolved d−d transitions, a low energy band at 15 400 cm^{-1}, and a higher energy absorption at 27 000 cm^{-1}: a shoulder is observed on the low-energy side of this second band, which is assumed to be the third d−d transition. To obtain the ligand-field parameters, the maximum and minimum values of this band were estimated: the parameters Δ_1, Δ_2, and B were calculated for these limiting values from the expressions previously derived. As can be seen from Table 6, the Racah parameter, B, is very sensitive to changes in the energy of this band, but the actual ligand-field splittings remain roughly constant. (A similar method was used in the calculation of parameters for $[CrCp^*_2]^+$.[36]) This assignment given is the only one that produced physically reasonable values of B. Similarly, the spectrum of $[CrCp^*Tp]^+[PF_6]^-$ displays three well-resolved bands of intensity consistent with spin-allowed d−d transitions. The parameters were calculated as above, again generating a physically reasonable value of B.

The striking feature arising from this simple analysis is that VCpTp and $[CrCp^*Tp]^+$ have Δ_1 values significantly larger than those observed for their metallocene analogues, whereas the Δ_2 values are noticeably smaller. The overall ligand-field splitting ($\Delta_1 + \Delta_2$) for VCpTp (24400−25800 cm^{-1}) is larger than that observed for VCp_2 (21 350 cm^{-1}); similarly for $[CrCp^*Tp]^+$ (27 170 cm^{-1}) it is larger than in $[CrCp^*_2]^+$ (24 700−25 400 cm^{-1}).

d^6 Species. The spectrum of $FeCp_2$ has been the subject of many reports, and the findings are conveniently summarized by Warren.[9] Sohn, Hendrickson, and Gray have also compared the spectra of the isoelectronic series $FeCp_2$, $RuCp_2$, and $[CoCp_2]^+$, and their findings form the basis of the following discussion.[68] For a $^1A_{1g}$ ($^1\Sigma^+$) metallocene three spin-allowed and three spin-forbidden transitions are predicted: the spin-allowed transitions, assignments, and ligand-field parameters for some known 18-electron species as well as for $[CoCp^*Tp]^+[PF_6]^-$, $[CoCpTp]^+[PF_6]^-$, $[CoCpTpm]^{2+}[PF_6^-]_2$, and $FeCp^*Tp$ are given in Table 7. To calculate the ligand-field splitting parameters, Δ_1 and Δ_2, using the expressions derived by Sohn et al. it is necessary to make an assumption about the ratio of the Racah parameters C and B.[68] For transition metal ions the relationship $C \approx 4B$ is found to be generally reasonable,[69] and for analysis of the spectra of metallocene species this ratio has been found to be satisfactory.[9] Hence it is also adopted in this work.

(68) Sohn, Y. S.; Hendrickson, D. N.; Gray, H. B. *J. Am. Chem. Soc.* **1971**, *93*, 3603−3612.

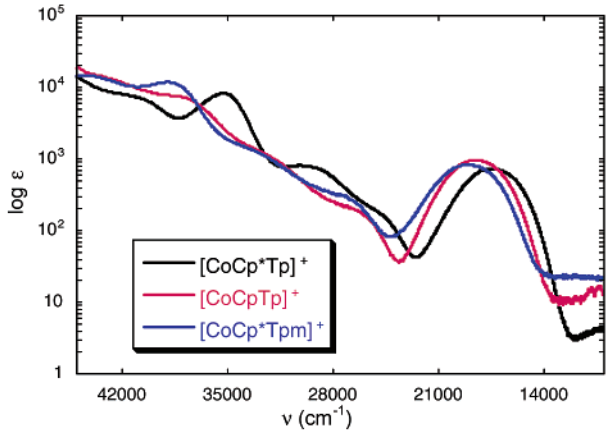

Figure 6. UV/visible spectra of $[CoCp^*Tp]^+$, $[CoCpTp]^+$, and $[CoCpTpm]^+$ as $[PF_6]^-$ salts in MeCN solution, plotted as log ϵ against energy (cm^{-1}).

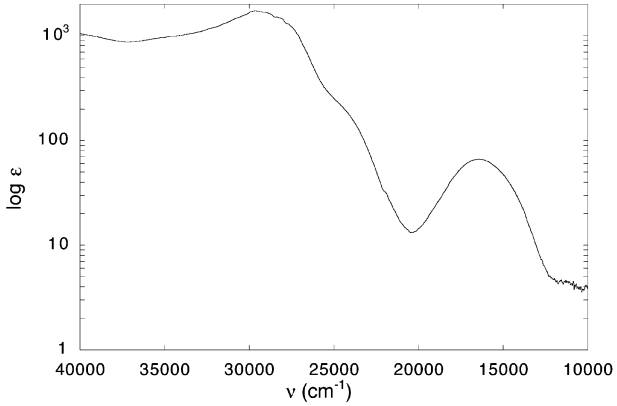

Figure 7. UV/visible spectra of FeCp*Tp in THF solution, plotted as log ϵ against energy (cm^{-1}).

The UV/vis spectra of the three Co(III) species above were all recorded in MeCN solution as $[PF_6]^-$ salts and as can be seen from Figure 6 are extremely similar. (The spectra of $[CoCpTp]^+$ and $[CoCpTpm]^{2+}$ as $[I]^-$ salts were also recorded and were superimposable with those with $[PF_6]^-$ anion, indicating no effect of counterion in these species.) They are characterized by a broad band at ~18 000 cm^{-1} and two overlapping bands between 24 000 and 33 000 cm^{-1}. The intensities of all three bands are suggestive of spin-allowed d−d transitions: extra features at higher energy are of intensity consistent with charge-transfer transitions. The positions of all three bands are well defined for $[CoCp^*Tp]^+$ and $[CoCpTp]^+$, but for $[CoCpTpm]^{2+}$ the highest energy transition is quite broad and thus the parameters were calculated for what are estimated to be the maximum and minimum energies for this band. As was found for VCpTp, *B* is sensitive to the position of this band, whereas the magnitudes of Δ_1 and Δ_2 are not greatly affected. In all cases the assignments as listed gave physically reasonable values of *B*, whereas the alternative assignment with the two higher energy bands transposed gave unreasonable (complex) values for *B*.

A noticeable feature of the spectra is that all three bands for $[CoCpTp]^+$ are to higher energy than those for $[CoCp^*Tp]^+$; the transitions for $[CpCoTpm]^{2+}$ are highest of all in energy. Therefore, both Δ_1 and Δ_2 values (and as a result the overall ligand-field splitting also) are larger for $[CoCpTp]^+$ than $[CoCp^*Tp]^+$; they are larger still for $[CpCoTpm]^{2+}$ consistent with it being a doubly charged rather than a singly charged cation. The difference between $[CoCpTp]^+$ and $[CoCp^*Tp]^+$ is somewhat counterintuitive when compared to the metallocenes where permethylation causes a significant increase in the energy of these d−d transitions and hence in the overall ligand-field splitting also (the increase on going from MCp_2 to MCp^*_2 is 5200 cm^{-1} for M = Fe and 6600 cm^{-1} for M = Co).[36] Almost all of this increase arises from greater δ-σ splitting (Δ_1), the σ-π (Δ_2) gap remaining roughly constant between MCp_2 and MCp^*_2. The total ligand-field splitting in $[CoCp^*Tp]^+$ (29 470 cm^{-1}) and $[CoCpTp]^+$ (30 650 cm^{-1}) is smaller than in both $CoCp_2$ (31 600 cm^{-1}) and $CoCp^*_2$ (38 200 cm^{-1}), which is predominantly a result of the much smaller values of Δ_2 in the mixed-sandwich species.

The spectrum of FeCp*Tp was recorded at room temperature in THF solution and is shown in Figure 7. As discussed earlier, FeCp*Tp shows solution NMR behavior consistent with a spin-equilibrium species. The optical spectrum of a spin-equilibrium complex in solution should be a superposition of the spectra expected for each spin-state isomer;[70] thus, in this case, it should consist of a superposition of the spectrum of the $^1\Sigma^+$ species (which should be similar to those described for the Co(III) species above) and that of the $^5\Delta$ species. For a high-spin d^6 system in axial symmetry, one transition is predicted in the UV/visible portion of the spectrum $^5\Delta \rightarrow {}^5\Pi$ (a much lower energy band should also be observed corresponding to an electronic transition within the σ and δ levels, $^5\Sigma^+ \rightarrow {}^5\Pi$).[9] The room-temperature d−d spectrum of FeCp*Tp is similar in form but shifted to slightly lower energy than the spectra of the Co(III) species. Here, the highest energy band is quite intense ($\epsilon \approx 2000$ mol^{-1} dm^3 cm^{-1}) and is therefore probably a charge transfer, rather than a d−d, band. In the HS species, the $^5\Delta \rightarrow {}^5\Pi$ transition is expected to lie at lower energy than any of the singlet transitions in the LS species; however, no such band is observed. It may be that the transitions of the LS species are inherently more intense than the HS transition, which is thus obscured. At this temperature, therefore, the spectrum is seemingly dominated by the LS form. Ligand-field calculations were performed for FeCp*Tp in the same way as for the Co(III) species, assuming that the highest energy band, $^1\Sigma^- \rightarrow {}^1\Pi$(b), is obscured by the transition at 29 000 cm^{-1}. The parameters were therefore calculated assuming maximum and minimum energies for this band of 30 000 and 26 000 cm^{-1}, respectively, as shown in Table 7. Again the value of *B* is very sensitive to the position of this band, but the splitting Δ_2 is only slightly affected. Δ_2 in FeCp*Tp is smaller than is observed in the Co(III) complexes and also approximately 6000−7000 cm^{-1} smaller than that calculated

(69) Huheey, J. H.; Keiter, E. A.; Keiter, R. L. *Inorganic Chemistry: Principles of Structure and Reactivity*, 4th ed.; HarperCollins: New York, 1993.

(70) Martin, L. L.; Martin, R. L.; Sargeson, A. M. *Polyhedron* **1994**, *13*, 1969−1980.

Table 8. UV−Vis Spectral Assignments and Parameters for Nickelocene Species[a]

	$^3A_2 \rightarrow {}^3E_{1g}(a)$; $^3\Sigma \rightarrow {}^3\Pi(a)$	$^3A_{2g} \rightarrow {}^3E_{2g}$; $^3\Sigma \rightarrow {}^3\Phi$	$^3A_{2g} \rightarrow {}^3E_{1g}(b)$; $^3\Sigma \rightarrow {}^3\Pi(b)$	Δ_1	Δ_2	B	β[f]
$NiCp_2$ [b]	14 380 (62)	16 900 (23)	23 450 (26)	4600	13 920	570	0.55
$NiCp^*_2$ [c]	15 900 (99)	18 500 (58)	25 000−26 500 (3250)[e]	4800	15 400	580	0.50
				4900	15 600	690	0.66
NiCpTp[d]	14 300 (230)	20 000 (210)	22 500 (340)	7780	13 140	305	0.29
NiCp*Tp[d]	12 200 (120)	19 200 (45)	24 000 (660)	10330	10 500	540	0.52

[a] All energies in cm^{-1}; extinction coefficients (mol^{-1} dm^3 cm^{-1}) are given in parentheses. [b] Data from ref 88; assignments from ref 9. [c] Data from ref 36. [d] This work. [e] Estimated minimum and maximum energies of this band. [f] Nephelauxetic ratio given by $B_{complex}/B_{free\ ion}$, where $B_{complex}$ is value listed and $B_{free\ ion}$ is the value in the gaseous transition metal ion as listed in ref 87.

for $FeCp_2$ and $FeCp^*_2$. The energies of the $^1A_{1g} \rightarrow {}^1T_{1g}$ transitions in low-spin $FeTp_2$ and $Fe[B(pz)_4]_2$ have been reported to be 18 700 and 18 900 cm^{-1}, respectively, whereas the $^5T_{2g} \rightarrow {}^5E_g$ transitions in low-spin $FeTp^*_2$ and $FeTp^{Me3}_2$ were both measured at 12 500 cm^{-1}.[14] By construction of the Tanabe−Sugano diagram for octahedral d^6 configuration, Δ_{HS} was estimated to be 12 500 cm^{-1} and Δ_{LS} to be 21 000 cm^{-1}, with a crossover point (i.e. interconversion between the two ground states) at 15 000 cm^{-1}.

d^8 Species. The d^8 case is very similar to that for d^3 species, with three one-electron spin-allowed transitions from the $^3\Sigma^-$ ground state to excited states denoted $^3\Pi(a)$, $^3\Phi$, and $^3\Pi(b)$. Warren has comprehensively examined the spectrum of $NiCp_2$ and has also assigned some spin-forbidden transitions; the energy ordering $^3\Pi(b) > {}^3\Phi > {}^3\Pi(b)$ was found to be the only physically reasonable solution to the ligand-field expressions.[9] The d−d spectrum of $NiCp^*_2$ was assigned similarly by Robbins and co-workers, although the highest energy d−d band is apparently hidden beneath a charge-transfer band.[36] The Racah parameter is quite sensitive to the position of this band; however, the value of Δ_2 changes much less significantly. Both Δ_1 and Δ_2 are calculated to be larger in the permethylated complex. The relevant data for these complexes are given in Table 8.

For NiCp*Tp and NiCpTp, the lowest energy bands are found at 12 200 and 14 300 cm^{-1}, respectively. Both are of intensity consistent with spin-allowed transitions. In both compounds, two further bands can be resolved as shoulders of charge-transfer transitions at 28 000 and 33 000 cm^{-1}, respectively. The intensities of these shoulders are again consistent with spin-allowed transitions, and the positions of both these bands have been estimated and are tabulated in Table 8. Calculation of the ligand-field parameters was performed using the expressions given by Prins and subsequently by Warren,[9,39] and the values are given in Table 8. Real values of B were obtained in both cases for assignments of the lowest energy band as $^3\Sigma^- \rightarrow {}^3\Pi(a)$, whereas complex values of B were obtained if this was assigned as $^3\Sigma \rightarrow {}^3\Phi$, i.e. with the σ-orbitals lower in energy than the δ. An interesting result from these calculations is that the overall ligand-field splittings in both complexes are almost identical (20 920 cm^{-1} for NiCpTp and 20 830 cm^{-1} for NiCp*Tp) and very similar to that determined for $NiCp^*_2$ (20 200−20 500 cm^{-1}) although somewhat larger than that for $NiCp_2$ (18 520 cm^{-1}). The splitting Δ_1 in both cases is substantially larger than in the metallocenes and significantly greater in NiCp*Tp than in NiCpTp, whereas Δ_2 is smaller in both cases than in the metallocenes.

Other Systems. Less information can be drawn from the spectra of the d^2 and d^4 species. Tanabe−Sugano diagrams for these configurations in axial symmetry have been given by Warren,[9] but in both cases we observed fewer bands than the number of spin-allowed transitions predicted. Also, in each case the crystal structure shows lower symmetry than axial and so further splittings are expected. However, the salient features are summarized for completeness. The optical spectrum of CrCp*Tp in THF is dominated by a single broad absorption at 18 500 cm^{-1} ($\epsilon = 345$ mol^{-1} dm^3 cm^{-1}), which overlaps on the high energy side with intense charge-transfer transitions. The UV/vis spectrum of $[VCpTp]^+$ in CH_2Cl_2 solution displays four bands (13 000 cm^{-1}, $\epsilon = 8$; 18 400 cm^{-1}, $\epsilon = 145$; 27 000 cm^{-1}, $\epsilon = 3000$; 31 000 cm^{-1}, $\epsilon = 5200$) to the low energy side of an intense charge-transfer band (40 500 cm^{-1}, $\epsilon = 11\,600$).

We have previously given the spectra of both CoCp*Tp and CoCpTp.[3] CoCp*Tp exists in solution in conformational equilibrium which hinders any meaningful interpretation of its spectrum which, in any case, is broad and relatively featureless. The spectrum of CoCpTp, by contrast, exhibits three well-resolved transitions of intensity consistent with spin-allowed d−d transitions. This is the predicted pattern for a high-spin d^7 system in axial ($^4\Delta$ ground state)[9] or octahedral symmetry ($^4T_{1g}$ ground state).[61] The band energies we observe correlate well with previous observations for octahedral high-spin Co(II) systems (collated by Banci et al.)[61] being at 10 800 ($\epsilon = 44$), 20 800 ($\epsilon = 178$), and 24 400 ($\epsilon = 414$) cm^{-1}, respectively, and the observed intensities are increased as a consequence of the lower symmetry. The electronic spectra of both complexes are therefore consistent with the different ground-state configurations implied by the magnetic data.

In summary, the spin-allowed d−d transitions can be assigned in a fashion similar to the metallocenes for the 15-, 18- (Co(III)), and 20-electron complexes. Ligand-field parameters were calculated and show that for 15-electron species the total ligand-field splitting, Δ_{TOT}, is larger than for their metallocene analogues, whereas for the 18-electron case Δ_{TOT} is smaller and for 20-electron systems Δ_{TOT} is approximately the same. In all cases, however, the value of Δ_2 is substantially reduced compared to the metallocenes, and in the majority of cases Δ_1 is markedly larger. In all cases the assignments gave positive values of Δ_1, i.e., putting the δ orbitals lower in energy than the σ orbitals. (This finding will be discussed in greater detail in the following

Table 9. Calculated Orbital Energies (eV) and Orbital Splitting Parameters for Ni Complexes with the Symmetry Labels Appropriate for D_{3d} ($NiTp_2$), C_s ($NiCp^RTp$), and D_{5d} ($NiCp^*_2$) Given for Each Level

	$NiTp_2$	NiCpTp	NiCp*Tp	$NiCp_2$	$NiCp^*_2$
π	$-3.99\ e_{1g}$	-3.90 A″	-3.38 A″	$-3.77\ e_{1g}$	$-2.86\ e_{1g}$
		-3.95 A′	-3.43 A′		
δ	$-5.59\ e_{1g}$	-5.35 A″	-4.90 A″	$-5.73\ e_{2g}$	$-5.01\ e_{2g}$
		-5.36 A′	-4.95 A′		
σ	$-6.29\ a_{1g}$	-6.18 A′	-5.66 A′	$-5.97\ a_{1g}$	$-5.24\ a_{1g}$
SD[a]	1.38	1.21	1.16	1.06	1.00
$\epsilon_\pi-\epsilon_\sigma$ [b]	2.30 (18 550)	2.26[c] (18 390)	2.27[c] (18 390)	2.20 (17 740)	2.38 (19 200)
$\epsilon_\pi-\epsilon_\delta$ [b]	1.60 (12 900)	1.43[c] (11 530)	1.52[c] (12 260)	1.96 (15 810)	2.15 (17 340)

[a] Spin density on the metal center. [b] Values in parentheses are in cm^{-1}. [c] Values calculated using the average energy of the near-degenerate π- and δ-levels.

section.) The nephelauxetic ratios generally indicate a slight increase in covalency from MCp^R_2 to MCp^RTp in all three cases.

DFT Calculations of Mixed-Sandwich Complexes MCp^RTp (M = V, Cr, Fe, Co and Ni). Density functional calculations were carried out on the mixed-sandwich complexes with two objectives. One was to obtain detailed information on the frontier orbitals of principally d character, their relative energies, and composition, how these changed as a function of the metal, and how they compared with the homoleptic analogues. The other was to gain insight into the structural distortions of the MTp fragment from C_3 symmetry found for $[VCpTp]^+$, CrCp*Tp, and CoCp*Tp.

Geometry optimizations were performed under symmetry constraints where reasonable. These were C_s for the mixed-sandwich compounds (which is the approximate symmetry of these species observed crystallographically),[2] D_{3d} for MTp_2, and D_{5d} for MCp^*_2. The C_s symmetry constraint was useful for the mixed-sandwich compounds as it assisted in fixing the configuration; this procedure was sometimes necessary for SCF convergence from near-degenerate ground states. Fragment calculations were used to calculate the contributions of the separate ligands and the metal to the frontier orbitals for selected molecules. In these the basis sets for a single point calculation on the molecule are the MOs generated by single point calculations on the ligands with the same geometry as they have in the optimized structure of the molecule.

The general procedure for modeling the structural distortions was to start from a C_s-symmetric structure for MCpTp with equal M−N distances, fix the configuration, and proceed to optimize the structure. The MCp*Tp analogue was then optimized by adding methyl groups to the MCpTp optimized structure, so as to maintain the C_s symmetry, and reoptimizing.

Orbital Energy Calculations. To gauge the characteristics of the ligand environment DFT calculations were performed on a series of 20-electron complexes, $NiTp_2$, NiCpTp, NiCp*Tp, $NiCp_2$, and $NiCp^*_2$. This series was chosen as each complex has two unpaired electrons, and its UV/visible spectrum has been studied and assigned. The structures of NiCp*Tp,[2] $NiTp_2$,[66] and $NiCp_2$ [67] were used for the input geometries for the mixed Cp^R/Tp and homoleptic sandwich complexes, respectively. The optimized structures were in excellent agreement with the experimental data. The largely metal-based d-orbital energies were calculated for all members of the series, from which the % metal contribution to these orbitals can be established. Table 9 lists the orbital energies and the orbital separations calculated from them, and Figure 8 gives a schematic of the energy levels. Further calculations were then performed to analyze the relative contributions of the Tp and Cp^R ligands to each of these orbitals for $NiTp_2$, NiCpTp, NiCp*Tp, and $NiCp^*_2$, and these results are detailed in Table 10.

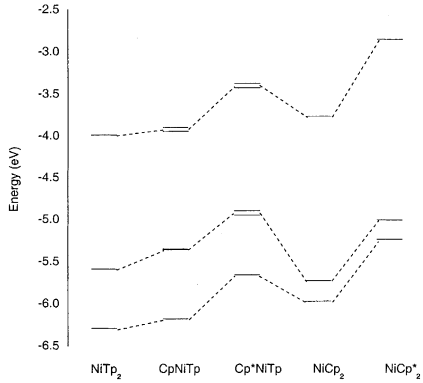

Figure 8. Schematic of the calculated d-orbital splittings in $NiCp^RTp$ complexes.

The calculated d-based orbitals of $NiTp_2$ and $NiCp^R_2$ are split into three sets of σ, δ, and π symmetry with respect to the principal molecular axis. For $NiCp^RTp$, the formal symmetry is C_s and as a consequence the degeneracy of the δ- and π-levels is lifted slightly; however, this is a small effect as the maximum such splitting is calculated to be 0.05 eV (ca. 400 cm^{-1}). Thus, the assumption of axial (or C_{3v}) symmetry seems reasonable. In all four cases the σ-orbital is calculated to lie lowest in energy. The overall d-orbital splitting, $\epsilon_\pi-\epsilon_\sigma$, is found to be largest for $NiCp^*_2$ but only slightly greater than for the other three complexes for which the values are all very similar. $\epsilon_\pi-\epsilon_\delta$ is smallest in the $NiCp^R$-Tp complexes. The spin density on the metal decreases in the order $NiTp_2$ > NiCpTp > NiCp*Tp > $NiCp_2$ > $NiCp^*_2$.

The calculations predict that in all three types of complex the σ-level is largely metal based with a Ni contribution of greater than 90%. For $NiCp^*_2$ the δ-levels also have predominantly metal character and thus remain essentially nonbonding; for the Tp-containing complexes, however, these orbitals have significant Tp character (ranging from 24% in NiCp*Tp to 44% in $NiTp_2$) and are moderately antibonding in character. The π-levels in all cases have

Table 10. DFT-Calculated Ligand and Metal Contributions to Metal-Based d-Orbitals in Ni(II) Complexes Given as %

	π			δ			σ		
	Ni	Tp	Cp^R	Ni	Tp	Cp^R	M	Tp	Cp^R
$NiTp_2$	53	47		54	44		96	1	
NiCpTp	41/41	16/17	42/41	61/60	31/32	5/5	92	0	3
NiCp*Tp	36/36	13/13	50/50	67/66	23/25	6/6	91	0	3
$NiCp^*_2$	30		69	93		5	96		1

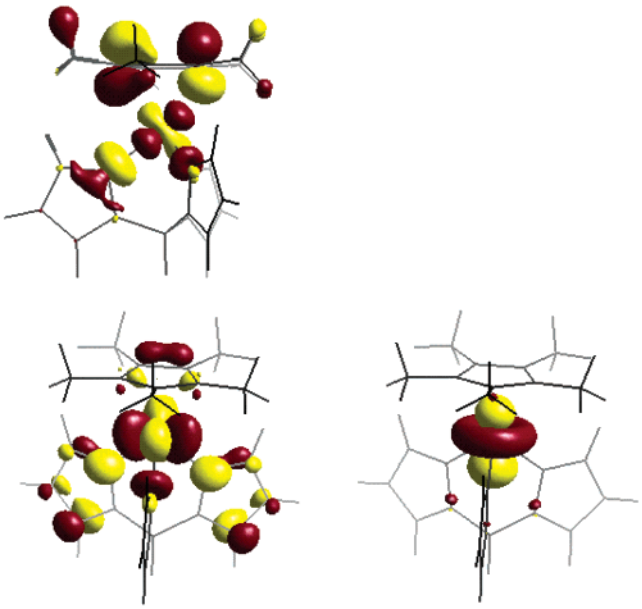

Figure 9. Isosurfaces of the metal-based σ-orbital (44A′) and one each of the near-degenerate pairs of δ (45A′) and π (46A′) orbitals, as calculated for NiCp*Tp.

considerable ligand character and are strongly antibonding, although the metal contribution increases on replacement of Cp^R by Tp.

Figure 9 shows a calculated orbital of each type for NiCp*Tp. The orbital of π-symmetry with respect to the principal axis (46A′) shows the Cp−Ni and Tp−Ni antibonding interactions: The Tp interaction results from overlap of σ-orbitals on the pyrazolyl rings (N "lone pairs"). The Tp−M antibonding interactions contributing to the orbital of δ-symmetry (45A′) with respect to the principal axis result from a combination of donation from both the pyrazolyl ring π-MOs (from two pyrazolyl rings) and σ-donation from a single N "lone pair" to the metal d-orbital of δ-symmetry. The orbital of σ-symmetry with respect to the principal axis (44A′) has overwhelmingly s and d_{z^2} metal character with little contribution from either ligand.

The trend in orbital splittings is readily explained by these observations. Thus, in all the Tp-containing complexes the δ-levels are raised relatively in energy, resulting in increased values of $\epsilon_\delta - \epsilon_\sigma$ and reduced values of $\epsilon_\pi - \epsilon_\delta$ compared with MCp^R_2. Cp* is a better π-donor than Cp, and thus orbital splittings are greater in MCp^*_2 species than in MCp_2. Tp is a moderate δ-donor as well as a good π-donor, whereas Cp^R is a better π-donor but a potential δ-acceptor. With a late transition metal such as Ni δ back-donation from the metal is minimal. It is important to note, especially for Tp, that these symmetry labels are with respect to the principal axis: Appropriate combinations of σ-type orbitals on the N atoms ("lone pairs") can form bonds of π-symmetry with respect to this axis to a metal; combinations of pyrazolyl-framework MO's and N "lone pairs" can form bonds of δ-symmetry with respect to this axis. These findings correlate well with the EHMO calculations of Curtis et. al. on $\{TpMo(CO)_3\}^\bullet$ and $\{CpMo(CO)_3\}^\bullet$ in which the contribution of the pyrazolyl ring π-orbitals in bonding to the metal was found to be significant also.[68] Fragment calculations on VpCpTp and $[VCpTp]^+$ gave similar orbital compositions (Table 11). These are discussed in more detail below.

Thus, the origin of the tendency to high-spin behavior is clear in these complexes. By comparison with the metallocenes, replacement of Cp^R for Tp to give a MCp^RTp complex results in a decreased energy gap between the two highest d-based levels ($\epsilon_\pi - \epsilon_\delta$ or Δ_2) as a consequence of the enhanced δ-donating properties of the Tp ligand. Thus, in the case of CrCp*Tp, CoCpTp, and FeCp*Tp (in solution) this must be sufficient to make the occupation of an antibonding π-level over a more weakly antibonding δ-level favorable with respect to the spin-pairing energy. The larger zero-field splitting parameter observed for NiCp*Tp over those of $NiCp_2$ and $NiCp^*_2$ can be attributed to a greater degree of metal character in the π-levels in this compound. This is borne out by the values calculated for the metal contributions to these orbitals and by the calculated spin densities on Ni detailed in Table 10.

There is a difference between the ligand-field d orbital ordering and that of the related Kohn−Sham orbital energies from the DFT calculations. Whereas the LFT analysis of the optical spectra results in $\delta < \sigma < \pi$, the DFT treatment gives $\sigma < \delta < \pi$.

Though this appears contradictory, it should be noted that ligand-field level energies give the energy of a d-electron in the field of the ligands and the metal core and do not include electron−electron repulsion between the d-electrons. Kohn−Sham one-electron energies, like ab initio orbital energies, include all electron−electron repulsion. It is well established that a similar reversal of δ and σ ordering occurs for $FeCp_2$. Though ligand field treatments put δ below σ for $FeCp_2$, $[FeCp_2]^+$ has the ground-state configuration $\sigma^2\delta^3$ as this configuration reduces the electron−electron repulsion.[89] Ab initio and DFT treatments, which include this factor in their orbital energies, calculate σ as more stable than δ. Due to this reversal in energy of the σ- and δ-levels between DF and LFT analysis, when there is reference to ligand-field splittings derived from DF calculations, the terminology $\epsilon_\pi - \epsilon_\delta$ and $\epsilon_\delta - \epsilon_\sigma$ is used; Δ_1 and Δ_2, as previously defined, refer to the splittings $\epsilon_\pi - \epsilon_\sigma$ and $\epsilon_\sigma - \epsilon_\delta$.

The most direct way of comparing the effect of the metal is to consider mixed-sandwich complexes with d^3, low-spin

Table 11. Summary of the Relative Energies of the DFT-Calculated σ, π, and δ Symmetry Frontier Orbitals in MCp^RTp Complexes

compd	$[VCpTp]^+$	VCpTp	CrCpTp	CrCp*Tp	FeCpTp	FeCp*Tp	$[CoCpTp]^+$	$[CoCp*Tp]^+$	CoCp*Tp[a]	NiCpTp	NiCp*Tp
d^n, S	2, 1	3, 3/2	4, 2	4, 2	6, 0	6, 0	6, 0	6, 0	7, 1/2	8, 1	8, 1
$\epsilon_\pi-\epsilon_\delta$	2.66	2.64	2.06	2.03	2.30	2.16	1.96	1.95	1.74	1.43	1.52
$\epsilon_\delta-\epsilon_\sigma$	0.37	0.28	0.45	0.47	0.58	0.60	1.25	1.06	0.71	0.82	0.74
$\epsilon_\pi-\epsilon_\sigma$	3.03	2.92	2.51	2.50	2.88	2.76	3.21	3.01	2.45	2.25	2.26

[a] Calculated structure for κ^3-Tp.

d^6, and d^8 complexes where structural distortions are not anticipated (vide infra) and the near degeneracy of the δ- and π-levels are maintained. The $\epsilon_\pi-\epsilon_\delta$ and $\epsilon_\delta-\epsilon_\sigma$ values for these are given in Table 11 together with those for d^2, d^4, and d^7 species. The values for the α spin orbitals are used, and an average value is taken for the δ- and π-levels. Throughout the series the level ordering is the same as for the Ni complexes discussed above.

Various trends are visible in the data summarized in Table 11. For the neutral complexes, the $\epsilon_\delta-\epsilon_\sigma$ values increase significantly across the transition series. This is largely a function of the stabilization of the predominantly metal σ-orbital with the increased nuclear charge. The larger $\epsilon_\delta-\epsilon_\sigma$ values for the monocations have the same origin. The $\epsilon_\pi-\epsilon_\sigma$ values are also largest for the cations in accord with ligand field expectations. Otherwise the trend in $\epsilon_\pi-\epsilon_\sigma$ values is less regular as might be expected from its dependence on configuration. Another interesting feature is that the $\epsilon_\pi-\epsilon_\sigma$ values are, in general, calculated to be larger for a particular MCpTp complex than for its Cp* analogue—this is most significant where M = Fe(II) and Co(III). This finding is in good agreement with the ligand-field splittings obtained from the UV/vis data for $[CoCp*Tp]^+$ and $[CoCpTp]^+$ discussed above. This suggests that previous failures to isolate FeCpTp and CrCpTp may not be a result of thermodynamic factors arising from smaller ligand-field splittings in Cp complexes compared to their Cp* analogues.[2] The greater steric hindrance of the metal center in Cp* (vs Cp) complexes may also play a role in kinetically stabilizing the MCp*Tp species to ligand-exchange reactions. For Co(II), the different spin states of CoCp*Tp and CoCpTp point to the Cp*/Tp combination generating the stronger ligand field. The size of the ligand-field splitting therefore appears to be a sensitive function of the metal and its oxidation state as well as the particular ligand combination employed.

Structure Calculations. Although crystallographic data obtained for a wide range of these complexes indicate essentially axial symmetry (as determined by Cp^R(centroid)−M−B (α) angles close to 180° and angles between the least-squares plane of the Cp^R ring and the three ligating N atoms (β) of 0°), three structures stand out as having substantial distortions away from these ideal parameters. CrCp*Tp is markedly distorted with 2 short and a single lengthened Cr−N bond.[2] VCpTp has a more subtle distortion with α = 172.4° and β = 5.3°; however, all three V−N bond lengths remain very similar.[2] CoCp*Tp does not contain a 3-coordinate Tp ligand at all but is in fact 2-coordinate.[2] All three of these complexes, on the basis of the axially symmetric bonding model described earlier, have Jahn−Teller unstable electronic configurations arising from single occupancy of the doubly degenerate π (CrCp*Tp $\sigma^1\delta^2\pi^1$, CoCp*Tp $\sigma^2\delta^4\pi^1$) or δ (VCpTp $\sigma^1\delta^1$) orbitals in axial symmetry. It was thus of interest to determine whether these distortions could be reproduced by calculation and their origins confirmed.

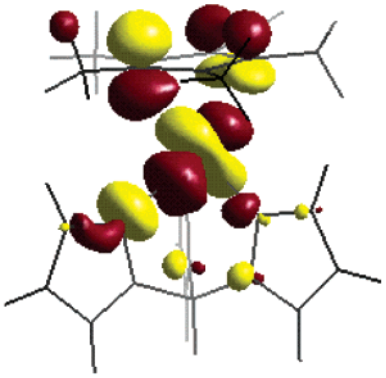

Figure 10. Calculated isosurface for the HOMO of CrCp*Tp.

Table 12. Comparison of Calculated and Observed Structural Data for CrCp*Tp and $[VCpTp]^+$

	CrCp*Tp		$[VCpTp]^+$	
	calcd	obsd	calcd	obsd
M−N (Å)	2.02	2.092(2)	1.980	2.055(3)
	2.02	2.123(2)	2.014	2.024(3)
	2.43	2.439(2)	2.014	2.059(3)
Cp(Ct)−M−N (deg)	120	117.1	121.2	121.2
	131	132.2	121.2	122.9
	131	134.2	133.2	132.7
α (deg)	163	167.4	172	172.4

For CrCp*Tp, geometry optimizations were performed with the spin of the Cr center fixed as $S = 2$. The calculations were found to reproduce the geometry of the complex well (this structure is described in more detail in ref 4), and some calculated and observed bond lengths and angles are given in Table 12. Variation in the Cr−C distances is also reproduced with short Cr−C distances of 2.26 Å and a long distance of 2.35 Å. The long Cr−C distance is found to lie to a carbon on the same side of the molecule as the long Cr−N distance, in agreement with the observed structure. The two d-orbitals of highest energy are derived from the antibonding orbitals of π-symmetry with respect to the principal axis; it is these levels which are unequally occupied in a high-spin d^4 sandwich molecule. The removal of the electronic degeneracy required by Jahn−Teller distortion leads to an energy-level splitting of 1.49 eV between these levels, hence, substantial stabilization of the HOMO. The calculated HOMO is depicted in Figure 10. The Tp−Cr overlap consists predominantly of an antibonding combination of a σ-orbital on one of the pyrazolyl rings (the N "lone pair") with a d-orbital of π-symmetry (with respect to the principal axis) but little interaction with the other two pyrazolyl rings, resulting in a single lengthened Cr−N bond. There is also substantial antibonding overlap between the

Table 13. DFT Calculated Orbital Energies and Ligand and Metal Contributions (as %) to Metal-Based d-Orbitals in $[VCpTp]^+$ and VCpTp

	$VCpTp^+$				VCpTp			
MO	energy (eV)	V(d)	Cp	Tp	energy (eV)	V(d)	Cp	Tp
π	−5.00	52.3	20.0	13.8	−0.52	64.1	16.0	14.2
π	−5.20	58.8	23.5	16.2	−0.55	62.2	17.9	15.0
δ	−7.59	68.2	7.5	19.6	−3.15	71.8	8.4	15.8
δ	−7.92	69.5	7.2	19.6	−3.18	71.5	8.0	15.6
σ	−8.13	88.6	0	0	−3.45	89.5	0	0

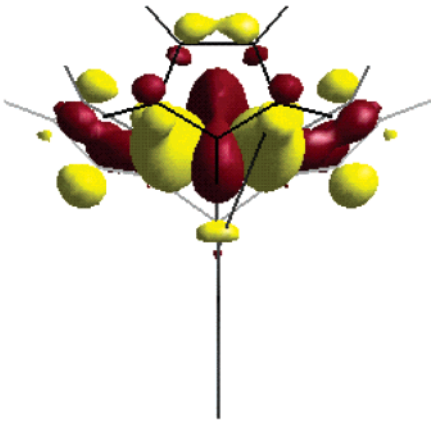

Figure 11. Calculated isosurface for the HOMO of $[VCpTp]^+$.

Cr-based orbital and a Cp* π*-level: unequal occupancy of the framework Cp π*-levels generates the crystallographically observed "ene"−"allyl" distortion in the Cp* ring.

For $[VCpTp]^+$ geometry optimizations were performed with the spin state of the V center fixed as $S = 1$. The calculation converged, and it was found that the distinctive features observed in the crystal structure were reproduced; in particular there was excellent agreement between the observed and calculated angles (Cp(centroid)−V−N and α) around the V center (see Table 12) which result in the characteristic "ring tilt" in the structure. Both the V−N and V−C both lengths are calculated to be slightly shorter than those observed, with slightly greater variation in the calculated V−C distances than those observed. (The observed cation does not contain crystallographically imposed mirror-plane symmetry).

Further calculations were then performed to calculate the relative contributions of the V, Cp, and Tp ligands to each of the calculated orbitals, in particular the frontier d-orbitals. These results are tabulated in Table 13. The lowest energy orbital is predominantly of V(d) origin and corresponds to the σ-orbital in axial symmetry. The degeneracy of the orbitals of δ- and π-symmetry in an axially symmetric scheme has been lifted; the splitting between the δ-symmetry orbitals is 0.33 eV (or 2700 cm^{-1}) and between the π is 0.20 eV (1600 cm^{-1}). Consistent with the previous observations from the Ni calculations, the δ-orbitals have significant Tp character (ca. 20% in the cation) but little Cp character (7%), whereas in the π-orbitals the contribution from Cp is important (20−23%) and the Tp contribution somewhat less so (14−16%). The δ HOMO is illustrated in Figure 11 and as it is symmetric with respect to the mirror plane results in a significant antibonding interaction with a single pyrazolyl ring, as in the Cr case. This interaction is dominated by the overlap of metal d-orbital with the MO derived from the pyrazolyl ring π-orbital rather than with the N "lone pair"; hence, the result of the distortion is to lift this ring out of the plane of the δ-orbital rather than to cause a dramatic bond lengthening as in the case of CrCp*Tp. The calculations therefore confirm a $\sigma^1\delta^1$ ground state, which due to the deviation from axial symmetry (large splitting of the δ-levels), is better thought of as an orbitally nondegenerate A′ ground state. This is therefore in good agreement with the magnetic measurements previously described, which are consistent with such a ground-state configuration.

Thus, in two cases where we predict Jahn−Teller type distortions from an axially symmetric MO scheme due to unequal occupancy of the hypothetically degenerate δ- and π-orbitals, sizable distortions are observed. We should therefore expect similar observations for electronic configurations that result also in unequal occupancy of these levels, for example low-spin d^7 (π^1), high- spin d^7, and low-spin d^5 (δ^3). As previously discussed, CoCp*Tp is an example of the former case and contains a 2-coordinate rather than a 3-coordinate Tp ligand. DFT calculations were performed on both 2- and 3-coordinate modes the coordination number being maintained by the symmetry constraint. The 2-coordinate species was found to be marginally more stable by 0.04 eV. The 3-coordinate structure showed a distortion with two Co−N distances of 1.93 Å and one lengthened bond of 2.196 Å. The splitting of the π-orbitals was 0.64 eV. The 2-coordinate structure had shorter Co−N distances of 1.88 Å, which are in reasonable agreement with the crystallographically determined distances of 1.931 Å.[2]

The high-spin d^7 case is fulfilled by CoCpTp, and crystallographic evidence points to a similar distortion in this molecule.[3] In this case the molecule lies on a crystallographic mirror plane (however, the geometry in this instance is staggered rather than eclipsed) and again the ring that lies in this plane is tilted away from the δ-plane with Cp(centroid)−Co−N of 129.6° vs 125.7° to the other two rings. The Co−N distance to this ring is somewhat shorter (2.069(2) Å vs 2.103(1) Å) also, and variation in the Co−Cp distances is also observed. The difference in bond angles and the deviation from linearity of α (177.4°) is somewhat smaller in this molecule than in $[VCpTp]^+$. This is not surprising though as the high-spin d^7 configuration requires occupancy of both the strongly antibonding π-levels, and we would expect distortions associated with unequal occupancy of the more weakly antibonding δ-levels to be somewhat masked as a result. Unfortunately, we have not isolated a complex which corresponds to the case in which there is a hole in the δ levels (low-spin d^5 $\sigma^2\delta^3$), but again we would expect such effects to be observed there also. In summary, Jahn−Teller effects have been observed in all

potentially Jahn−Teller unstable mixed-sandwich complexes—this is in contrast to the metallocenes in which distortion has only been observed in the high-quality crystal structure of $MnCp^*_2$.

Conclusion

The magnetochemistry, EPR, and electronic spectra of mixed Cp^R/Tp sandwich complexes have been compared with those of their metallocene and MTp_2 analogues. The electronic structures of the different classes of compounds have also been compared using DFT calculations. A consistent picture emerges whereby the $\sigma-\delta$ gap is decreased in the MCp^RTp complexes vs MCp^R_2, due to the δ-donating properties of the Tp ligand. This additional bonding interaction (with respect to Cp) raises the energy of the δ-levels and results in a tendency to high-spin complexes. An axially symmetric ligand-field model is consistent with the properties of complexes with orbitally nondegenerate configurations. However, unequal occupancy of both δ- and π-levels leads to substantial distortions from pseudoaxial symmetry that are easily observed crystallographically and yields effective nondegeneracy of the ground state in the case of $[VCpTp]^+$.

Experimental Details

All compounds were prepared by the routes previously described.[2]

Magnetic Susceptibility Measurements. Solid-state magnetic susceptibility data were obtained using a Quantum Design MPMS-5 SQUID magnetometer. Accurately weighed powdered samples of ca. 50 mg were loaded into gelatine capsules in a glovebox and placed between additional gelatine capsules in a nonmagnetic plastic straw, which was then lowered into the cryostat. Thus, the sample is mounted in a weakly diamagnetic medium and no correction need be made for the diamagnetism of the sample holder. The field independence of the susceptibility data was verified by measuring the susceptibility as a function of field between −5 and 5 T. Data were then measured employing fields of 0.1 and 0.5 T and were corrected for the inherent diamagnetism of the sample either by use of Pascal's constants[74] or by extrapolation of the susceptibility to infinite temperature.

Solution phase magnetic moments were measured using Evans' NMR method in C_6D_6 or toluene-d_8 [75] and moments calculated using the modified expression for a high-field superconducting magnet.[76,77]

EPR Spectroscopy. EPR spectra were recorded on microcrystalline solids, solutions, or glasses sealed in high-purity Spectrosil quartz tubes fitted with Young's type concentric stopcocks. An X-band Varian spectrometer fitted with a liquid- helium cryostat was used at an operating field of ca. 0.33 T. Spectra were referenced using a microcrystalline sample of K_3C_{60} ($g = 2.008$).[78]

Optical Spectroscopy. UV/visible spectra were recorded using a GBC Cintra 10 UV−visible spectrometer (range 186−1021 nm) as solutions of known concentration in THF, CH_2Cl_2, or MeCN using 1 cm quartz cells. Spectra of air-sensitive solutions were recorded using a quartz cell fitted with a sidearm sealed by a Rotaflo tap.

Computational Methods. Calculations were performed using density functional methods of the Amsterdam Density Functional Package (ADF 1999, ADF 2000.2).[79−82] Type IV basis sets were used with triple-ζ accuracy sets of Slater type orbitals, with a single polarization function added to the main group atoms. The cores of the atoms were frozen up to 2p for Cr, Co, and Ni and 1s for C and N. The local density approximation of Vosko, Wilk, and Nusair[83] was used with the nonlocal exchange corrections by Becke[84] and nonlocal correlation corrections by Perdew.[85]

Acknowledgment. We thank the EPSRC for support (T.J.B.) and Dr. S. Barlow for many helpful discussions.

IC030073U

(71) Bandoli, G.; Clemente, D. A.; Paolucci, G.; Doretti, L. *Cryst. Struct. Commun.* **1979**, *8*, 965−970.
(72) Seiler, P.; Dunitz, J. D. *Acta Crystallogr., Sect. B* **1980**, *B36*, 2255−2260.
(73) Curtis, M. D.; Shiu, K.-B.; Butler, W. M.; Huffman, J. C. *J. Am. Chem. Soc.* **1986**, *108*, 3335−3343.
(74) O'Conner, C. J. *Prog. Inorg. Chem.* **1982**, *29*, 203−283.
(75) Evans, D. F. *J. Chem. Soc.* **1959**, 2003−2005.
(76) Woolcock, J.; Zafar, A. *J. Chem. Educ.* **1992**, *69*, A176−A179.
(77) Schubert, E. M. *J. Chem. Educ.* **1992**, *69*, 62.
(78) Denning, M. D. Phil. Thesis, University of Oxford, 2000.
(79) Baerends, E. J.; Ellis, E. G.; Ros, P. *J. Chem. Phys.* **1973**, *2*, 41.
(80) Baerends, E. J.; Berces, A.; Bo, C.; Boerringter, P. M.; Cavallo, L.; Deng, L.; Dickson, R. M.; Ellis, D. E.; Fan, L.; Fischer, T. H.; Fonseca Guerra, C.; van Gisbergen, S. J.; Groeneveld, J. A.; Gritsenko, O. V.; Harris, F. E.; van den Hoek, P.; Jacobsen, H.; van Kessel, G.; Kootstra, F.; van Lenthe, E.; Osinga, V. P.; Philipsen, P. H. T.; Post, D.; Pye, C. C.; Ravenek, W.; Ros, P.; Schipper, P. R. T.; Schreckenbach, G.; Snijiders, J. G.; Sola, M.; Swerhone, D.; te Velde, G.; Vernooijis, P.; Versluis, L.; Visser, O.; van Wezenbeek, E.; Wiesenekker, G.; Wolff, S. K.; Woo, T. K.; Ziegler, T. ADF Program System Release 1999, Amsterdam, 1999.
(81) te Velde, B.; Baerends, E. J. *J. Comput. Phys.* **1992**, *99*, 84.
(82) Fonseca Guerra, C.; Snijider, J. G.; te Velde, G.; Baerends, E. J. *Theor. Chem. Acc.* **1998**, *99*, 391.
(83) Vosko, S. H.; Wilk, L.; Nusair, M. *Can. J. Phys.* **1990**, *58*, 1200.
(84) Becke, A. D. *Phys. Rev.* **1988**, *A38*, 2398.
(85) Perdew, J. P. *Phys. Rev. B* **1986**, *33*, 7046 and 8822.
(86) Pavlik, I.; Cerny, V.; Maxova, E. *Collect. Czech. Chem. Commun.* **1972**, *37*, 171−195.
(87) Lever, A. B. P. 2nd ed.; Elsevier: New York, 1986.
(88) Pavlik, I.; Cerny, V.; Maxova, E. *Collect. Czech. Chem. Commun.* **1970**, *35*, 3045−3063.
(89) Evans, S., Green, M. L. H., Jewitt, B., Orchard, A. F., Pygall, C. F. *J. Chem. Soc., Faraday Trans. 2* **1972**, 1874.